Available online at www.sciencedirect.com
ScienceDirect
Journal of volcanology and geothermal research
Journal of Volcanology and Geothermal Research 160 (2007) 263–284
www.elsevier.com/locate/jvolgeores

Pre-eruptive and syn-eruptive conditions in the Black Butte, California dacite: Insight into crystallization kinetics in a silicic magma system

Molly C. McCanta [a,*], Malcolm J. Rutherford [a], Julia E. Hammer [b]

[a] Department of Geological Sciences, Brown University, Box 1846, Providence, RI 02912, USA
[b] Department of Geology and Geophysics, University of Hawaii, 1680 East–West Road, Honolulu, HI 96822, USA

Received 7 April 2006; received in revised form 26 August 2006; accepted 3 October 2006
Available online 28 November 2006

Abstract

A series of experiments and petrographic analyses have been run to determine the pre-eruption phase equilibria and ascent dynamics of dacitic lavas composing Black Butte, a dome complex on the flank of Mount Shasta, California. Major and trace element analyses indicate that the Black Butte magma shared a common parent with contemporaneously erupted magmas at the Shasta summit. The Black Butte lava phenocryst phase assemblage (20 v.%) consists of amphibole, plagioclase (core $An_{77.5}$), and Fe–Ti oxides in a fine-grained (<0.5 mm) groundmass of plagioclase, pyroxene, Fe–Ti oxides, amphibole, and cristobalite. The phenocryst assemblage and crystal compositions are reproduced experimentally between 890 °C and 910 °C, ≥300 MPa, $X_{H2O}=1$, and oxygen fugacity = NNO + 1. This study has quantified the extent of three crystallization processes occurring in the Black Butte dacite that can be used to discern ascent processes. Magma ascent rate was quantified using the widths of amphibole breakdown rims in natural samples, using an experimental calibration of rim development in a similar magma at relevant conditions. The majority of rims are 34±10 μm thick, suggesting a time-integrated magma ascent rate of 0.004–0.006 m/s among all four dome lobes. This is comparable to values for effusive samples from the 1980 Mount St. Helens eruption and slightly faster than those estimated at Montserrat. A gap between the compositions of plagioclase phenocryst cores and microlites suggests that while phenocryst growth was continuous throughout ascent, microlite formation did not occur until significantly into ascent. The duration of crystallization is estimated using the magma reservoir depth and ascent rate, as determined from phase equilibria and amphibole rim widths, respectively. Textural analysis of the natural plagioclase crystals yields maximum growth rates of plagioclase phenocryst rims and groundmass microlites of 8.7×10^{-8} and 2.5×10^{-8} mm/s, respectively. These rates are comparable to values determined from time-sequenced samples of dacite erupted effusively from Mount St. Helens during 1980 and indicate that syneruptive crystallization processes were important during the Black Butte eruptive cycle.

Keywords: amphibole breakdown; arc magmatism; magma ascent; plagioclase growth; Mount Shasta

1. Introduction

Magmas erupted in arc regions are generally the products of a combination of processes that occur at depth in mid-crust level magma storage zones and during ascent to the surface. The compositional variability of many arc

* Corresponding author. Now at Lunar and Planetary Institute, Houston, TX 77058, USA. Tel.: +1 281 486 2118; fax: +1 281 486 2162.
E-mail address: McCanta@lpi.usra.edu (M.C. McCanta).

0377-0273/$ - see front matter © 2006 Elsevier B.V. All rights reserved.
doi:10.1016/j.jvolgeores.2006.10.004

magmas are clearly controlled by storage zone processes, such as mixing, assimilation, and crystal accumulation (e.g., Hammer et al., 2002; Pichavant et al., 2002; Rutherford and Devine, 2003). However, many also exhibit textural and compositional features that are the result of processes, such as magma degassing and syneruptive crystallization, that occurred in the conduit during transit to the surface (e.g., Cashman, 1992; Rutherford and Hill, 1993; Blundy and Cashman, 2005). Recognizing the distinction between processes active in the storage zone and those active during ascent to the surface is important as chamber conditions represent the initial conditions for eruption, while conduit processes may alter the course of an eruption in progress.

In order to understand and quantify the effects of the different processes outlined above on the observed eruptive products, the unique characteristics of each process need to be identified. A common approach to this problem is to first characterize the phenocryst-melt assemblage that existed at depth in the crustal magma storage zone and then to define the storage zone conditions necessary to recreate the assemblage through a combination of natural sample analyses and experiments (e.g., Rutherford and Devine, 1988; Rutherford et al., 1998). Once the equilibration conditions have been determined, changes that took place during ascent can be studied (Rutherford and Hill, 1993; Geschwind and Rutherford, 1995). However, many magmas contain phenocrysts with highly zoned crystals, raising questions as to which assemblage represents chemical equilibrium with the melt prior to final ascent (e.g., Blundy and Cashman, 2001; Pichavant et al., 2002; Hammer and Rutherford, 2003). Additionally, the effects of ascent processes may be complicated by reinjection or remobilization of magma just prior to or during eruption (Pallister et al., 1996; Rutherford and Devine, 2003).

In this study we examine the Black Butte dacite, an exceptionally homogeneous magma that appears to have escaped complicating processes such as re-injection. Previous work on the Black Butte dome eruption near Mount Shasta in northern California (Williams, 1932; Miller, 1978) suggested that, due to its textural and compositional homogeneity and simple eruptive history, the pre-eruption magmatic intensive conditions could be accurately characterized. Therefore it should be possible to identify the pre-eruption equilibrium phase assemblage and to determine the changes that took place during the final magma ascent to the surface. Further, it may be possible to evaluate these changes in terms of ascent path and rate, particularly if experimental simulations are combined with data from the natural samples.

The pre-eruptive magma storage zone conditions including temperature, pressure, oxygen fugacity (f_{O2}), and water content (X_{H2O}) were determined using new analytical data and appropriate thermobarometers. However, it is impossible to determine the magmatic equilibration conditions through petrographic analysis alone because the groundmass is holocrystalline and the Fe–Ti oxides exhibit subsolidus oxidation. Therefore, phase equilibrium experiments utilizing a natural sample as a starting composition were performed in order to simulate the crystallization sequence of the Black Butte magma and evaluate the natural magma storage zone conditions.

Our objectives were to determine the conditions present in the magma storage region at Black Butte during phenocryst crystallization and to investigate the compositional changes taking place during ascent and decompression of a phenocryst-bearing, water-rich dacitic magma. The Black Butte eruption is unique among similar effusive eruptions (i.e., 1980 Mount St. Helens, 1995 Soufriere Hills, Montserrat) for its extremely homogeneous composition and phase assemblage. The dome lobes represent an opportunity to integrate information from several crystal texture indicators of ascent rate: amphibole breakdown, plagioclase phenocryst growth, and microlite formation. The textural and chemical changes occurring in the magma during ascent were investigated in complementary studies of natural and experimental products. The phase equilibrium experiments not only establish the initial conditions prior to magma decompression, but, in tandem with analyses of the natural crystals, help constrain intensive conditions during ascent. Petrographic measurements of the widths of amphibole breakdown rims in the Black Butte dacite produced by decompression and the concomitant reduction in the H_2O content of the surrounding melt were used to estimate ascent rates following Rutherford and Hill (1993) and Rutherford et al. (1998). In addition, plagioclase composition changing in response to the evolving matrix melt during ascent (e.g., Geschwind and Rutherford, 1995) was used to interpret the relative timing of nucleation events and to evaluate rates of crystal growth. Black Butte provides a valuable test of the application of a variety of analytical methods in order to more completely understand crystallization processes taking place prior to and during an effusive eruption.

2. Geologic setting

Black Butte, a flank vent of Mount Shasta in the California arc volcanic system, consists of a series of four overlapping dacite dome lobes, distinguishable topographically (Fig. 1; R. Christiansen, unpublished

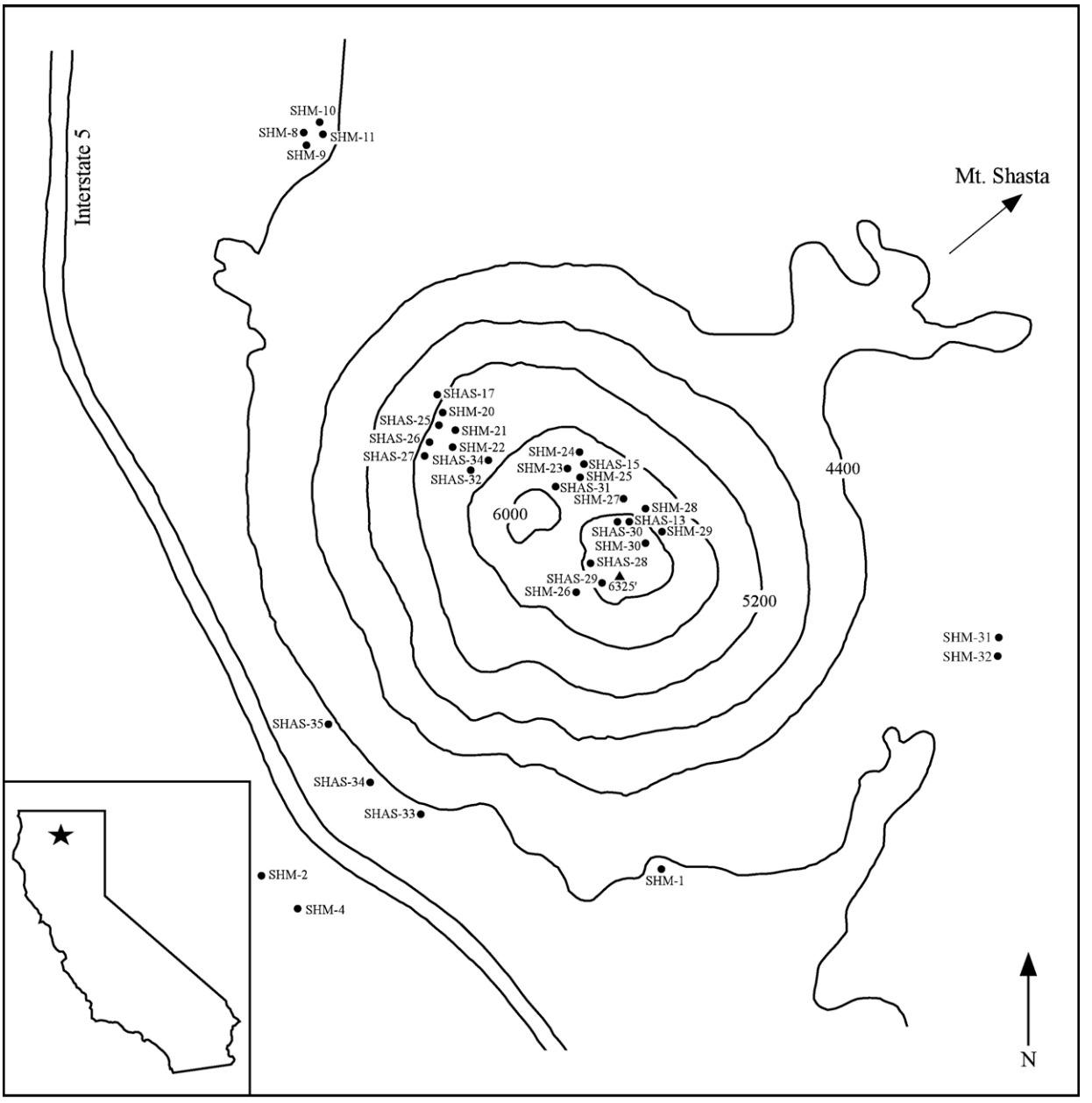

Fig. 1. Sample location map for Black Butte. Contour elevations are given in feet. The inset map shows the location of Black Butte in California.

data). The vent consists of a conical, multipeaked complex 10 km southwest of Mount Shasta erupted about 10,000 years B.P. (Miller, 1978). The peak rises 1938 m above sea level and contains approximately 1 km^3 of erupted material. The Black Butte eruptive sequence appears to have been contemporaneous with that which produced the Shastina cone, a chemically similar dacitic eruption from the main Shasta vent (Miller, 1978). The Black Butte phase assemblage is relatively simple; phenocrystic amphibole (≤2 cm), plagioclase (≤1.5 cm) and rare titanomagnetite (≤1 mm) in a completely crystalline groundmass of plagioclase, low-Ca and high-Ca pyroxenes, Fe–Ti oxides, and cristobalite. Although separate dome lobes are expressed topographically, there are no chemical or mineralogic variations within or among the lobes to suggest they are the product of multiple eruptive episodes. The phenocrysts, which make up 20% of the erupted magma are compositionally unzoned except for thin (≤20 μm) overgrowth rims on the plagioclase;

breakdown rims of ≤50 μm occur on all amphiboles. Flow lineation is present at both the macroscale, as evidenced by the preferred orientation of rod-shaped phenocrysts (Fig. 2A, B), and the microscale, seen in the preferred orientation of microlites in the groundmass (Fig. 2G). This eruption appears to represent tapping of

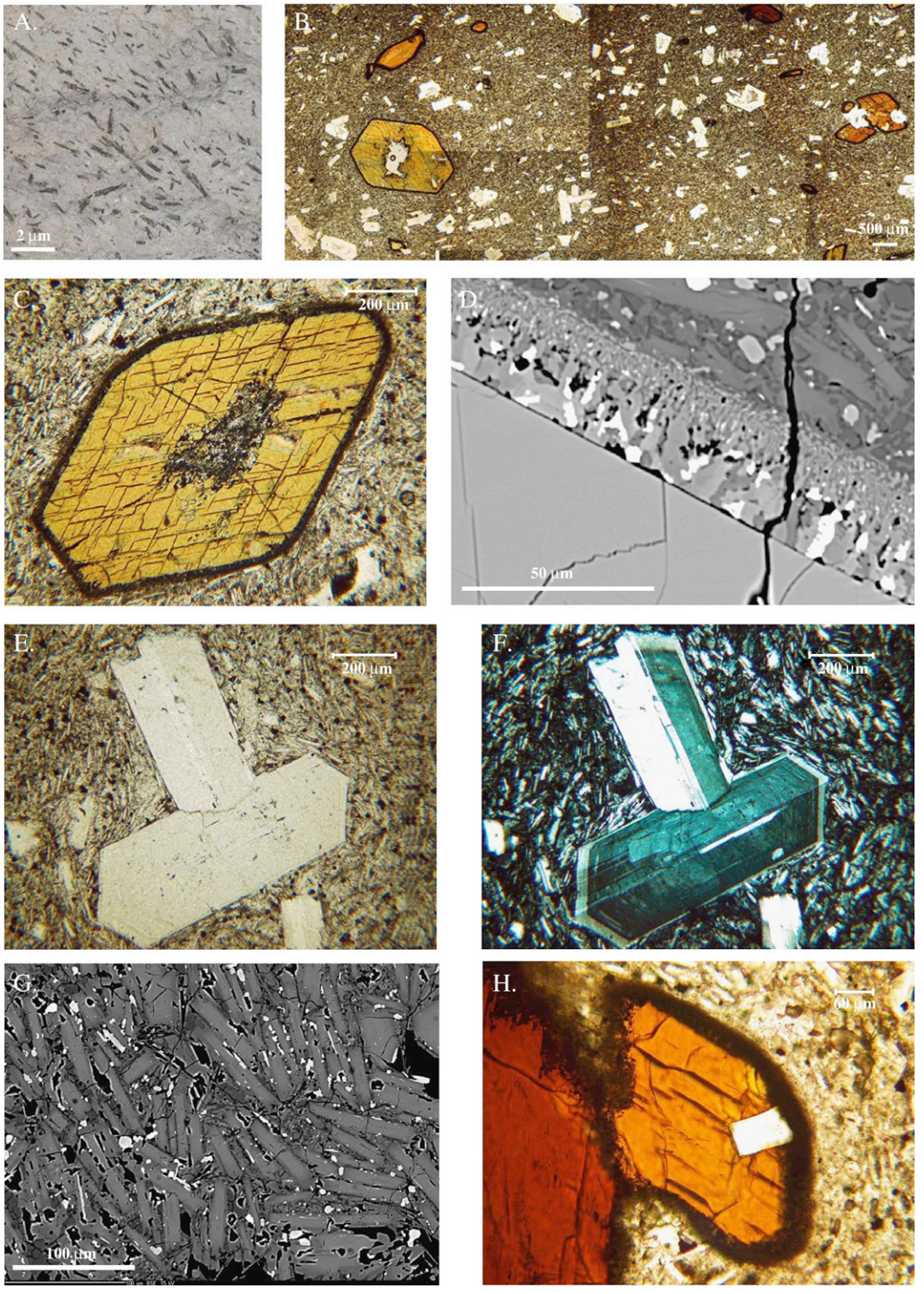

Table 1
Average composition of Black Butte phases. Major element totals are recorded as oxide weight percent. Trace element totals are recorded as parts per million. Numbers in parentheses indicate the standard deviation among sample analyses. NM indicates that the element was not analyzed

	Black Butte bulk rock [a]		Shastina Bulk Rock		Calculated groundmass [b]		Amphibole core		Plagioclase phenocryst core		Plagioclase phenocryst rim		Plagioclase microlite	
SiO_2	64.63	(0.17)	64.57	(0.06)	67.73	(0.67)	44.95	(0.20)	48.51	(0.26)	52.69	(0.62)	54.84	(1.07)
TiO_2	0.42	(0.01)	0.50	(0.02)	0.32	(0.04)	1.56	(0.10)	NM	–	NM	–	NM	–
Al_2O_3	17.24	(0.10)	16.89	(0.14)	17.42	(0.26)	11.38	(0.16)	32.81	(0.25)	29.77	(0.48)	28.33	(0.70)
FeO [c]	3.15	(0.10)	3.29	(0.02)	2.98	(0.56)	11.12	(0.25)	0.39	(0.02)	0.46	(0.03)	0.49	(0.05)
MgO	2.11	(0.10)	3.13	(0.11)	1.6	(0.26)	15.83	(0.12)	NM	–	NM	–	NM	–
CaO	5.15	(0.20)	5.99	(0.04)	4.22	(0.18)	11.56	(0.06)	15.94	(0.30)	12.25	(0.32)	10.49	(0.80)
Na_2O	4.63	(0.08)	4.21	(0.07)	4.46	(0.15)	1.92	(0.05)	2.32	(0.13)	4.25	(0.29)	4.94	(0.39)
K_2O	1.12	(0.04)	1.05	(0.07)	1.27	(0.07)	0.21	(0.01)	0.04	(0.02)	0.12	(0.04)	0.36	(0.07)
MnO	0.04	(0.02)	0.06	(0.01)	NM	–	0.13	(0.01)	NM	–	NM	–	NM	–
Cr_2O_3	NM	–	NM	–	NM	–	0.03	(0.02)	NM	–	NM	–	NM	–
Total	98.49		99.68		100.00		98.68		100.00		99.54		99.45	
La	3.2	(0.3)	4.3	(0.3)	Modal Analysis [d]		Si [e]	6.43	An	77.1	An	58.4	An	49.8
Ce	7.2	(0.6)	9.7	(0.6)	Gm	80	Al^4	1.58	Ab	22.5	Ab	40.5	Ab	46.8
Nd	3.1	(0.3)	4.2	(0.3)	Plag	16	Ti	0.17	Or	0.4	Or	1.1	Or	3.4
Sm	0.7	(0.1)	0.8	(0.1)	Amph	4	Al^6	0.34						
Dy	0.5	(0.1)	0.5	(0.1)			Cr	0						
Er	0.5	(0.0)	0.5	(0.1)			Fe^{3+}	0.33						
Yb	0.3	(0.0)	0.3	(0.0)			Fe^{2+}	1						
Li	20.6	(6.2)	10.6	(0.5)			Mg	3.37						
Be	1.2	(0.1)	0.9	(0.1)			Ca	1.77						
B	8.5	(1.6)	10.2	(3.9)			Mn	0.02						
Cr	12.5	(1.7)	82.5	(0.4)			Na	0.53						
Rb	15.3	(3.1)	15.1	(0.1)			K	0.04						
Sr	809.8	(41.8)	1045.9	(3.3)			Mg#	77.1						
Y	6.6	(0.2)	7.8	(0.5)										
Zr	79.3	(2.0)	77.5	(2.4)										
Nb	4.3	(0.7)	15.7	(4.6)										
Ba	226.1	(14.2)	199.9	(3.6)										

[a] Average analyses and standard deviation calculations for all four Black Butte lobes.
[b] Groundmass calculated utilizing mass balance relations. Data in parentheses are the standard deviations between multiple thin section calculations.
[c] All Fe as FeO.
[d] Modal analysis was conducted by point counting utilizing ~2000 points counted per thin section (four thin sections total). Analysis given in % material. Gm = groundmass; Plag = plagioclase; Amph = amphibole.
[e] Structural formula calculated after Robinson et al. (1982; HB15CT).

a single magma reservoir, in that there is no petrographic evidence for pre-eruptive mixing events (e.g., inversely zoned or partially resorbed phenocrysts).

Samples were collected from the surface and interior of each of the four dome lobes of Black Butte, as well as from pyroclastic flow material in the area around the dome (Fig. 1). Surface and interior samples were distinguished by color differences resulting from syn- and post-eruption oxidation. Surface samples generally appear pink due to post-eruption oxidation. Interior

Fig. 2. Images of the various phases in the Black Butte assemblage. Note the scale differences between the images. A. Photograph of Black Butte in hand sample. Evident are lineated dark amphibole phenocrysts in a grey matrix. B. Photomicrograph mosaic of the Black Butte phase assemblage in transmitted light. Note the large plagioclase and rimmed amphibole phenocrysts, the plagioclase–amphibole intergrowth, the small oxide microphenocrysts, and the completely crystalline groundmass. C. Transmitted light micrograph of Black Butte amphibole surrounded by a breakdown rim of reaction products. D. BSE image of a Black Butte amphibole breakdown rim. Note the coarse-grained (gabbroic) inner rim and the fine-grained (opacite) outer rim. E. Plane light photomicrograph of Black Butte plagioclase phenocrysts. F. Photomicrograph of the plagioclase phenocrysts from Fig. 1E in cross polars. G. BSE image of the Black Butte groundmass showing flow lineation of plagioclase microlites. H. Transmitted light micrograph illustrating the intergrowth of plagioclase and amphibole phenocrysts indicating co-crystallization.

samples retain their fresh, gray color (Fig. 2A). All samples were located utilizing an unpublished geologic map of the region provided by R. Christiansen.

3. Methods

3.1. Experimental

All experiments were performed in the experimental petrology laboratory at Brown University. The bulk compositions of the natural samples were determined by electron microprobe analysis. Splits of a 2 g rock powder sample were wrapped in Mo-foil packets, which were sealed in evacuated SiO_2-glass tubes and held at 1350 °C for 10 h to create a homogeneous glass. This method for obtaining a representative glass from a rock powder is well established for samples of this size (Rutherford et al., 1985). All forward (melting) experiments were run on powdered samples of SHAS-13, a representative Black Butte dome sample (an average bulk rock composition and standard deviation based on 10 samples of the four domes is given in Table 1). The utility of using the bulk composition for the crystallization study of the natural magma was demonstrated with initial experiments in which the natural phase assemblage was reproduced. A split of this material was fused under water-saturated conditions for 24 h at 950 °C and 200 MPa to create a water-rich starting glass for reversal (crystallization) experiments. For a subset of experiments both forward and reversal experiments were run at the same time in adjacent capsules to assist in evaluating the degree of equilibration in the run products (e.g., Hammer et al., 2002). Major element analyses of experimental glasses and phenocrysts (composition and abundance) from the dual runs were used to verify that crystal-melt equilibrium was attained at each set of run conditions.

All experimental charges were run in $Ag_{70}Pd_{30}$ tubes under the following conditions: T=800–950 °C, P_{total}=100–450 MPa, X_{H2O}=1, and f_{O2}=NNO+1 or NNO+2 (Table 2). Distilled water was added to the sample tubes in sufficient quantity to saturate the melts with an H_2O-rich fluid at the desired pressure. Experiments were run in three types of pressure vessels. Experiments at temperatures from 825–880 °C and pressures ≤250 MPa were conducted in cold-seal Waspaloy pressure vessels, with water as the pressurizing medium. Experiments at temperatures above 880 °C and pressures ≤250 MPa were run in titanium–zirconium–molybdenum (TZM) pressures vessels, using a mixture of Ar+CH_4 gases as the pressurizing medium. Experiments at pressures of 300 MPa and above were run in an internally heated pressure vessel (IHPV) with a mixture of H_2+Ar gases as the pressurizing medium. Pressures were measured using pressure transducers periodically checked against a factory-calibrated Heise gauge and are accurate to ±2 MPa. Run temperatures are accurate to ±5 °C based on periodic checks against the Au melting temperature.

Oxygen fugacity in the experimental samples was varied using either gas mixing or solid buffer assemblages. In the TZM and IHPV runs, the f_{O2} was buffered using gas mixing equilibria as described by Eugster and Skippen (1967). The f_{O2} was monitored with solid buffer assemblages of either (Ni–NiO)+1 (NNO+1) or Re–ReO_2 (f_{O2}=NNO+2), contained in unsealed tubes adjacent to the sample (e.g., Eugster, 1957, 1959; Frost, 1991). In experiments run in Rene vessels, the f_{O2} was controlled by inserting Ni-rods into the vessel, buffering the f_{O2} at NNO+1 (±0.5 log units) (Geschwind and Rutherford, 1992). The f_{O2} values were chosen based on values recorded in similar magmatic systems (i.e., Mount St. Helens) and Fe–Ti oxide measurements in compositionally similar samples from Shastina (NNO+0.5–2.5) (Lawson et al., 1987).

Crystallization experiments run separate from melting experiments were held at temperatures 25 °C above the final run temperature for 24 h to ensure melt homogenization and were then cooled at 5 °C/h to the desired run temperature. This prevented rapid nucleation of many small crystals and allowed for the growth of larger crystals. Run durations ranged from 2 days to 4 weeks to achieve crystal-melt equilibrium (Table 2). Samples were isobarically quenched at the end of each experiment. When opening a run capsule, the presence of water and both buffer components were verified to confirm that the desired experimental conditions were maintained. Samples that did not meet these criteria were discarded. Sample chips were mounted, sectioned, and polished. Sections were examined optically prior to electron microprobe analysis. Experimental conditions and run products are summarized in Table 2.

3.2. Analytical

Natural and experimental samples were analyzed and imaged on the Brown University Cameca Camebax and SX-100 electron microprobes and American Museum of Natural History SX-100 electron microprobe. Glass analyses were obtained using a 15 kV acceleration voltage, 10 nA beam current, a defocused beam (diameter=5–15 μm), beam blanking between points, and a correction for sodium loss during analysis using the online correction scheme and method of Nielsen and

Table 2
Experimental run conditions and run products. gl = glass; plag = plagioclase; amph = amphibole; opx = orthopyroxene; cpx = clinopyroxene; oxd = Fe–Ti oxide

Run	T (°C)	P (MPa)	f_{O2}	Duration (h)	Run products
MC-59	825	100	NNO+1	120	gl, plag, opx, cpx, oxd
MC-57	850	100	NNO+1	48	gl, plag, opx, cpx, oxd
MC-56	900	100	NNO+1	720	gl, plag, opx, cpx, oxd
MC-27	825	150	NNO+1	672	gl, plag, amph, opx, cpx, oxd
MC-26, 29	850	150	NNO+1	528, 504	gl, plag, amph, opx, cpx, oxd
MC-25, 28	875	150	NNO+1	504, 504	gl, plag, amph, opx, cpx, oxd
MC-22	900	150	NNO+1	48	gl, plag, opx, cpx, oxd
MC-8	950	150	NNO+1	48	gl
MC-52	800	200	NNO+1	336	gl, plag, amph, opx, cpx, oxd
MC-51	825	200	NNO+1	312	gl, plag, amph, opx, cpx, oxd
MC-49	850	200	NNO+1	456	gl, plag, amph, opx, cpx, oxd
MC-45	850	200	NNO+2	96	gl, plag, amph, opx, cpx, oxd
MC-44	875	200	NNO+2	48	gl, plag, amph, opx, cpx, oxd
MC-48	875	200	NNO+1	48	gl, plag, amph, opx, cpx, oxd
MC-53	900	200	NNO+1	48	gl, plag, opx, cpx, oxd
MC-79	925	200	NNO+1	12	gl, plag, oxd
MC-46	950	200	NNO+1	48	gl
MC-24	825	300	NNO+1	192	gl, plag, amph, opx, cpx, oxd
MC-30	850	300	NNO+1	96	gl, plag, amph, opx, cpx, oxd
MC-68	850	300	NNO+1	96	gl, plag, amph, opx, cpx, oxd
MC-70	870	300	NNO+1	48	gl, plag, amph, opx, cpx, oxd
MC-33	875	300	NNO+1	48	gl, plag, amph, opx, cpx, oxd
MC-76	875	300	NNO+1	12	gl, plag, amph, opx, cpx, oxd
MC-69	900	300	NNO+1	48	gl, plag, amph, oxd
MC-75	900	300	NNO+1	12	gl, plag, amph, oxd
MC-74	870	350	NNO+1	12	gl, plag, amph, opx, cpx, oxd
MC-73	870	400	NNO+1	12	gl, plag, amph, cpx, oxd
MC-80	900	420	NNO+1	10	gl, plag, amph, oxd
MC-71	900	450	NNO+1	24	gl, amph

Sigurdsson (1981). Minerals were analyzed for major element composition using a 15 kV acceleration voltage, 15 nA beam current, and a focused beam (diameter=2–5 μm). Natural mineral standards were used for calibration. Bulk rock rare-earth and other trace-element data was collected on the Woods Hole Oceanographic Institution Cameca IMS 3f ion microprobe. A 15–20 μm beam with a 90 V offset was used. A dacitic glass from Mt. St. Helens was used as the analysis standard (N. Shimizu, personal communication).

Amphibole breakdown rim widths were measured using an Olympus petrographic microscope and reflected light, following the procedures of Rutherford and Hill (1993). Multiple samples collected from different locations on each dome were used to make amphibole rim width measurements. Individual rim width measurements consisted of measuring the rim in four places along the perimeter of a single crystal and computing an average rim width for that phenocryst. The variance in the four measurements per phenocryst was used to estimate measurement error. Rutherford and Hill (1993) estimated error on a single phenocryst rim to be 2 μm for a 10 μm thick rim (±20% relative) and 5 μm for a 40 μm thick rim (±12% relative). A conservative rim width error estimate of ±20% was applied to the Black Butte amphibole rim measurements.

Plagioclase phenocryst rims were identified using back scatter electron (BSE) images and measured using electron microprobe traverses. Both BSE images and microprobe data show clear breaks between the uniform phenocryst core composition and zoned rim composition. Phenocryst traverses were made in numerous thin sections from all four Black Butte dome lobes.

Plagioclase phenocryst, microphenocryst, and microlite textural analyses were performed on photomicrographs and BSE images of samples cut parallel to the groundmass flow lineation, respectively. This was done in an attempt to minimize any cut effects, i.e. the ability to bisect the true center of a crystal, which may influence the measurement of the "core" composition of the crystal. Images were acquired from a minimum of eight different locations of each thin section. The photomicrographs

were collected at a magnification of 5× and the BSE images were collected at a magnification of 500× to account for the size differences between the phenocryst, microphenocryst, and microlite populations. Analysis of the width, length, aspect ratio, flow direction, and plagioclase composition were made on a minimum of two thin sections from each sample location (Fig. 1). Two sample locations were analyzed for lobes 1, 2, and 4. Due to its small area of exposure, only one sample from lobe 3 was analyzed. Approximately 400 phenocrysts in each section were measured. Combined BSE images for each thin section studied yielded approximately 400 microlites for textural measurements, a subset of which were also analyzed using the electron microprobe. Textural analyses were completed both manually and using the software package "NIH Image". Images were manually thresholded and converted to binaries with this software package. Microlite number density and best-fitting ellipse dimensions were then computed. The textural data was used to compute shape corrected crystal size distributions (CSD) using the method described in Hammer et al. (1999). Distributions were determined separately for the high magnification and low magnification data sets resulting in CSDs that overlapped by ~50 μm.

4. Results

4.1. General petrology and mineralogy

The Black Butte eruptions produced a series of dacitic lava dome lobes as well as a large apron of block and ash flow debris covering an area of 44 km^2 (Miller, 1978). The exposed dacite ranges from massive lava dome samples to slightly vesicular pyroclastic blocks. No pumiceous material is associated with the eruption that formed Black Butte. The Black Butte phase assemblage consists of flow-lineated plagioclase (≤1.5 cm) and amphibole phenocrysts (≤2 cm) and smaller Fe–Ti oxide phenocrysts (≤1 mm) in a high silica, microcrystalline groundmass (<0.5 mm) (Fig. 2A, B). Phenocryst melt inclusions are rare. The sparse, small holocrystalline inclusions that do exist are typically intersected by cracks suggesting the potential for volatile loss. Volumetric mineral modes were determined by point counting two thin sections per each of the four lobes at approximately 2000 points per thin section. The groundmass composes 80±2% of the Black Butte lavas. The remaining 20% consists of phenocrystic plagioclase (16±2%), amphibole (4±1%), and titanomagnetite (<1%). The groundmass is composed of flow-aligned microlites of plagioclase interspersed with Fe–Ti oxides, cristobalite, and acicular Ca-rich and Ca-poor pyroxenes. There are no discrete glass pools in the groundmass and vesicles are sparse (1–2% fine vesicles) in the majority of samples.

4.1.1. Bulk rock composition

The electron microprobe analyses of the fused natural powders indicate that, within analytical uncertainty, all Black Butte dome lobes are identical in composition (Table 1). They are classified as dacites in the classification scheme of Le Bas et al. (1986) and are indistinguishable from dacite samples erupted contemporaneously at Mount Shasta. Additionally, this bulk rock composition plots along the same major element covariation trend as other Shasta samples (Fig. 3). The whole rock trace element compositions of Black Butte lobe lavas and coeval (Miller, 1978) pyroclastic samples from Mount Shasta (Shastina) are identical within analytical uncertainty (Table 1). The similarity of both major and trace elements in the bulk rock compositions strongly suggests that the lavas of Black Butte and Shastina were derived from a common Mount Shasta magmatic system (Table 1).

4.1.2. Amphibole phenocrysts

Black Butte amphibole is classified as tshermakite (Leake et al., 1997). Phenocrysts are euhedral, reddish-brown in color, unzoned, and are invariably surrounded by a 19–59 μm thick rim of breakdown products (Fig. 2C, D). The crystals range up to ~2 cm along the *c*-axis. The elongate amphibole crystals are aligned by magma flow, imparting a strong lineation to the rocks (Fig. 4). The lack of rim material on crystal faces in contact with other phenocrysts indicates that the breakdown involved amphibole reaction with melt. The breakdown of amphibole takes place during magma ascent and depressurization when the melt water content is no longer sufficient to stabilize amphibole and follows the reaction amphibole + $melt_1$ ↔ orthopyroxene + clinopyroxene + plagioclase + ilmenite + $melt_2$ (Rutherford and Hill, 1993; Browne and Gardner, 2004). The widths of amphibole reaction rims can be used to estimate ascent rate (Rutherford and Hill, 1993). The distribution of rim widths within individual samples yields information on the velocity distribution in the upper conduit. Thus, the variance of amphibole rim widths (Fig. 2D) among Black Butte dome lobes should reflect the variability of ascent rates throughout the eruption. Histograms of amphibole rim widths are given in Fig. 5. Natural rim widths range from 19 to 59 μm. The distributions of rim widths, particularly the maxima, of samples from lobes 1 and 4 are slightly greater than those samples from lobes 2 and 3 (Fig. 5B–E).

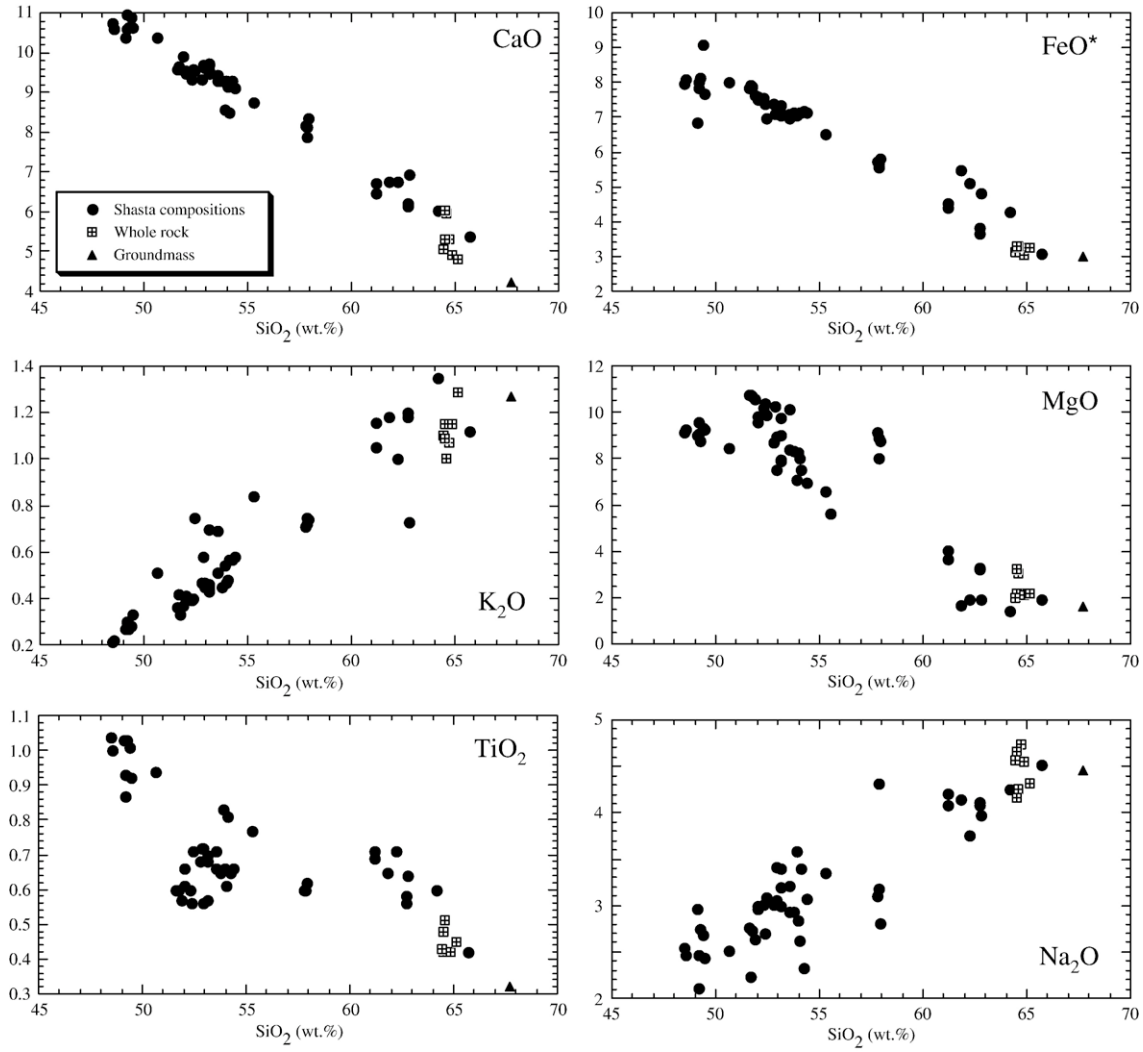

Fig. 3. Harker diagrams illustrating the compositional range of Mount Shasta rock types and their relationship to the Black Butte magmas. Data on Shasta rock compositions (circles) from Smith and Carmichael (1968), Condie and Swenson (1974), Baker et al. (1994), and Bacon et al. (1997). Black Butte dacitic bulk-rock composition (crossed squares) and calculated groundmass (triangle) from this study.

In addition to the coarse-grained decompression-induced breakdown rims, a fine-grained opacite layer occurs on the outer edge of the coarse-grained reaction products and fills many cracks in the amphibole phenocrysts (Fig. 2D). This opacite portion of the rim is variable in thickness and very fine grained (<1 μm). Unlike the decompression rims, which occur only where the amphibole was in contact with melt, indicating a melt role in the breakdown reaction, the opacite material both rims and crosscuts the amphibole phenocrysts. These rims are distinctly different from the breakdown rims produced through amphibole reaction with the melt during decompression. Garcia and Jacobson (1979) refer to the decompression-breakdown rims (measured above) as the "gabbroic" type and the opacitic rims as the "black" type. They suggest a decrease in magmatic f_{H2O} as the origin for the gabbroic (decompression) rims, which was later confirmed experimentally by Rutherford and Hill (1993) and a syn- or post-eruption oxidation–dehydrogenation origin for the black rims. The late-stage development of the opacite does not appear to have any consistent relationship to the width of the rims produced by decompression reaction (Fig. 2D).

4.1.3. Plagioclase phenocrysts

The lath-to tabular-shaped, euhedral plagioclase phenocrysts in the Black Butte phase assemblage range in size up to 1.5 cm in length (Fig. 2E, F). Microprobe traverses across individual plagioclase grains width-wise show large cores with uniform

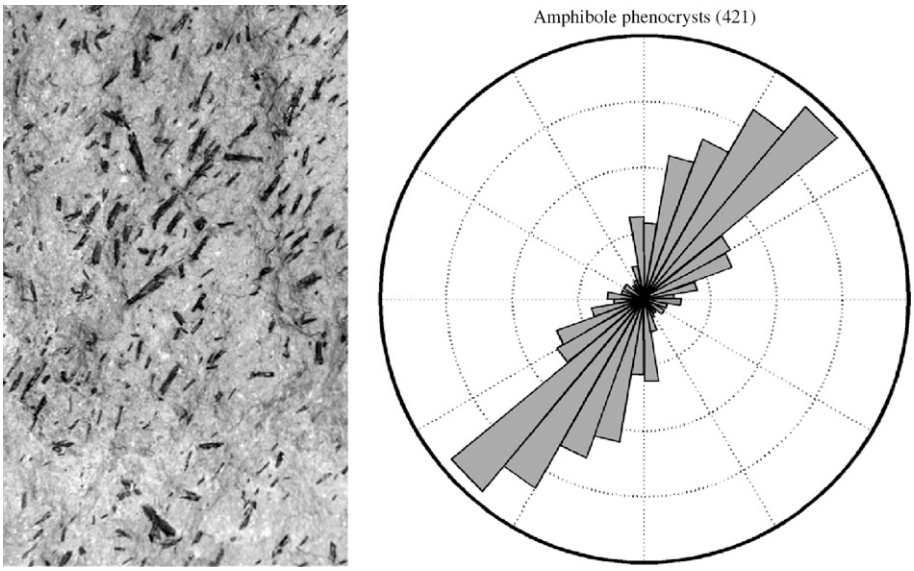

Fig. 4. Rose plot illustrating the strong orientation of amphibole phenocrysts as seen in the accompanying photograph. Number in parentheses is the number of analyses used in the plot.

compositions averaging $An_{77.5\pm1.4}$ (Figs. 6 and 7A). Rims are zoned from $An_{77.5}$ to $An_{39.8}$ (Fig. 6). The normally-zoned plagioclase rims average 17±3 μm in width. The break between the uniform composition plagioclase cores and the zoned rims is apparent in BSE images (Fig. 6). Approximately 15% of the plagioclase phenocrysts exhibit sieve-textured cores suggesting they are relict crystals from an early magma mixing event, potentially in the greater Shasta magmatic system. This sieve texture may be caused by resorption of the plagioclase suddenly out of equilibrium with the surrounding melt prior to growth of a different composition (e.g., Tsuchiyama, 1985). All sieve-textured cores are enclosed by thick unzoned mantles of non-sieve-textured plagioclase. These mantles have the same high-An cores to low-An rim patterns as observed in plagioclase grains without sieved cores. Additionally, plagioclase grains trapped inside amphibole crystals (e.g., Fig. 2H) are homogeneous, have average compositions of $An_{74.5\pm4.4}$, and lack the normally-zoned rim.

4.1.4. Plagioclase microphenocrysts

Microphenocrysts are defined here as crystals with widths ranging from 50–150 μm. Plagioclase microphenocrysts are predominantly homogeneous, lath-shaped grains. Their core compositions cluster in the range An_{52} to An_{62}, although some show core compositions up to An_{77} (Fig. 7B). Cut effect issues may account for some of the scatter. Electron microprobe traverses across some of the largest microphenocrysts show normal compositional zonation similar to that exhibited by the rims of the plagioclase phenocrysts. The microphenocrysts appear closely related to the phenocryst population in zonation and texture, with size being the distinguishing factor.

4.1.5. Plagioclase microlites

Microlites (Fig. 2G) are defined here as crystals ≤50 μm in width. Plagioclase microlites are primarily homogeneous, lath-shaped grains that exhibit strong flow lineation (Fig. 8). These crystals are consistently less An-rich than the phenocryst cores. The microlites range in composition from An_{30} to An_{62}, similar to the outer-most phenocryst rim composition (Fig. 7A). The plagioclase microlite population has core compositions that do not exceed $An_{62.0}$ (Fig. 7B). This is in stark contrast to the cores of the plagioclase phenocrysts discussed in the above section which have compositions averaging $An_{77.5\pm1.4}$ and whose rims are normally zoned to $An_{39.8}$. These compositional differences suggest two distinct populations of plagioclase coexist in the Black Butte dacite, presumably reflecting nucleation and growth at different times, extents of effective undercooling, and different intensive parameter conditions.

The presence of two distinct plagioclase crystal populations is also supported by size distribution data. Phenocryst, microphenocryst, and microlite width frequencies are shown on log-linear CSD (e.g., Marsh, 1988) diagrams (Fig. 9). Two lines are required to adequately fit both the phenocryst (both macro and

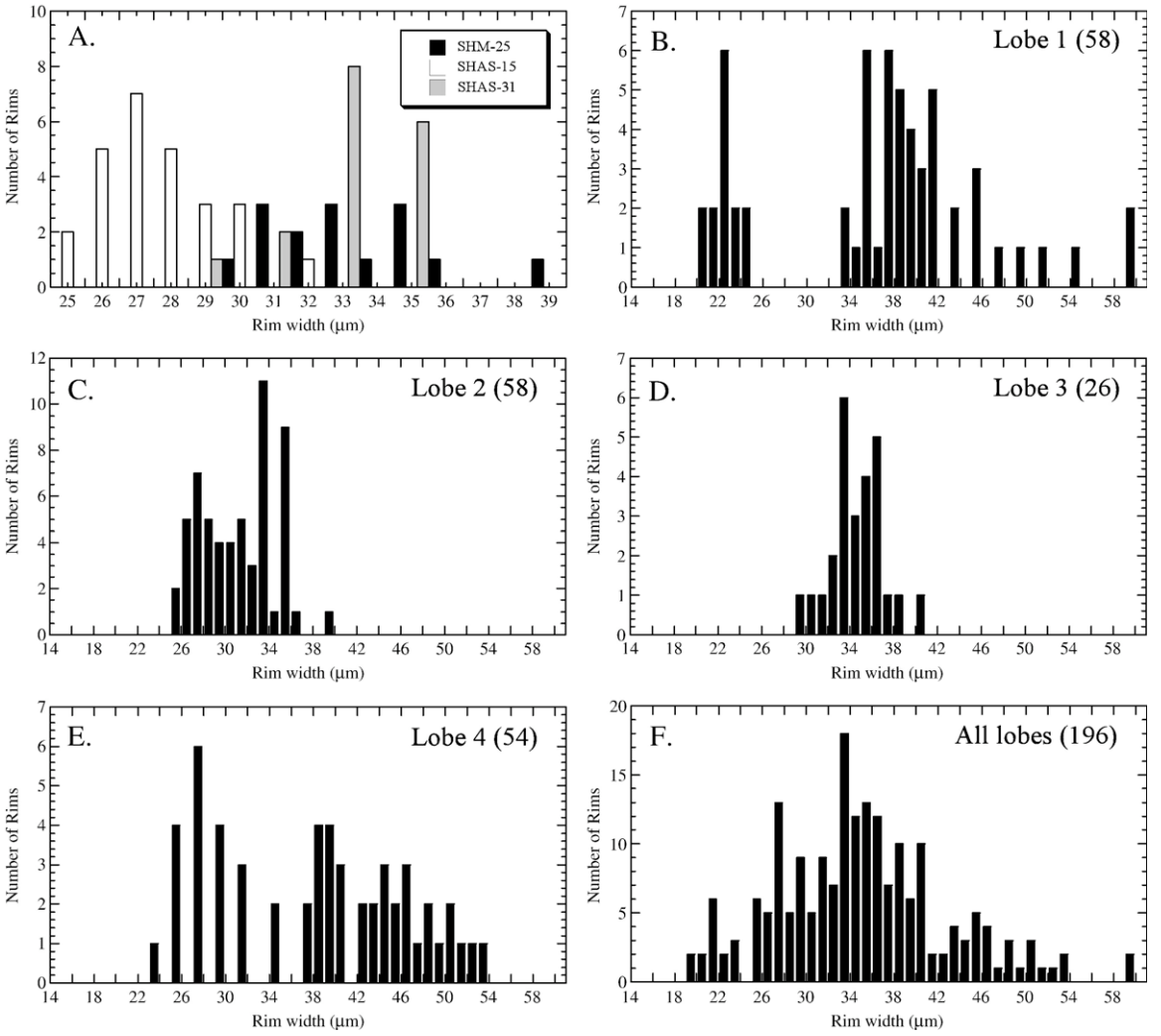

Fig. 5. Histograms of amphibole breakdown reaction rim widths measured in the Black Butte samples from this study and B. Katz, unpublished data. Numbers in parentheses are the number of analyses used in each histogram. A. Data from three separate thin sections all from lobe 2. Rim width variations occur from sample to sample, but within a single sample the range of rim widths is small. This is in comparison to amphibole rim widths in the Mt. St. Helens 1980 dacites, which ranged from 0–60 μm in single thin sections (Rutherford and Hill, 1993). B. All rim widths measured in lobe 1 (n=58). C. All rim widths measured in lobe 2 (n=58). D. All rim widths measured in lobe 3 (n=26). E. All rim widths measured in lobe 4 (n=54). F. Rim width data for all four dome lobes. Note the distinct peak at 34±10 μm.

micro) and microlite data. The cutoff width that defines the two populations is approximately 40 μm. A slight upward curvature in the low magnification data suggests coarsening or gently accelerating nucleation. The sensitivity of the bin size selection on the calculated slopes and intercepts was evaluated and it was determined that the slope and intercept values change by less than a few percent as the bin size was varied. A comparison was made between the linear fits to the data to evaluate crystal growth regimes. Notably, each lobe contains two distinct crystal populations, indicated by a sharp break in slope in the CSD (Fig. 9). We interpret the size distribution and compositional data presented above to indicate that plagioclase growth occurred under two different regimes, one in the magma storage region and one during ascent.

4.1.6. Groundmass

The Black Butte groundmass is composed of flow-aligned microlites of plagioclase interspersed with Fe–Ti oxides, cristobalite, amphibole, and acicular pyroxenes (Fig. 2G). Groundmass crystallization in the lavas is nearly complete, leaving essentially no identifiable glass and sparse vesicles. Although a melt composition could

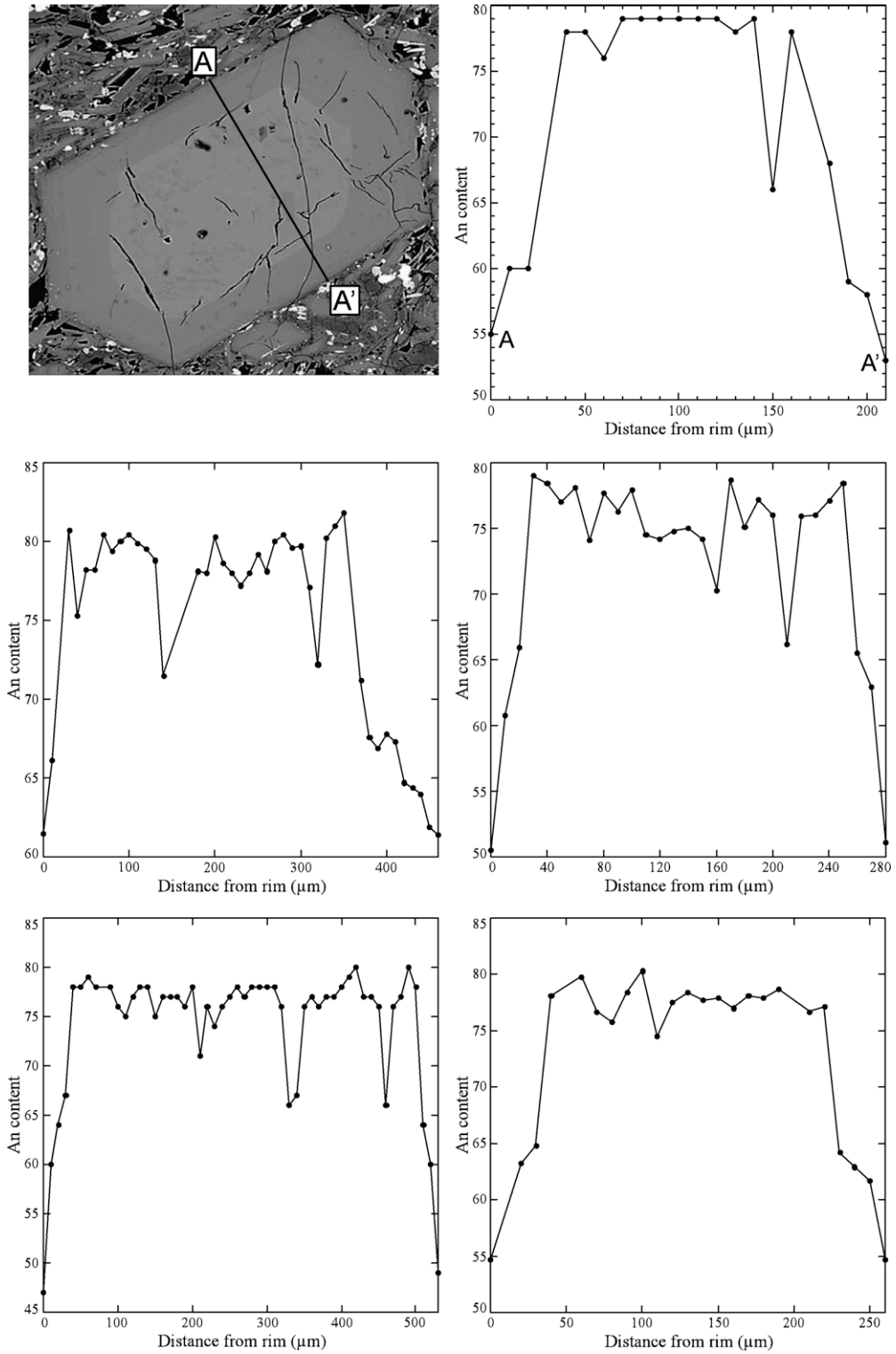

Fig. 6. BSE image of a plagioclase phenocryst and the corresponding electron microprobe traverse A to A′. Also shown are traverses across four additional phenocrysts of different sizes. Note the zoned rims, ~An_{78} to ~An_{55}, surrounding the homogeneous cores in all traverses. Excursions to lower An values in the cores reflect imperfections in the samples, such as cracks or inclusions, primarily of melt.

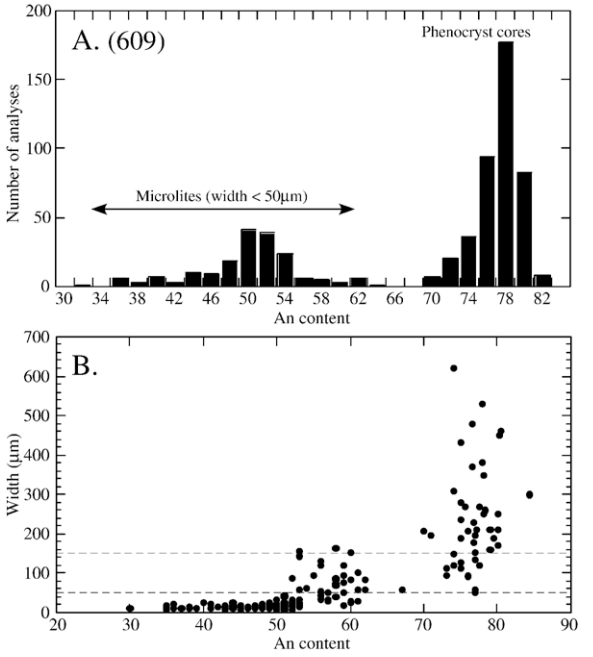

Fig. 7. A. Histogram comparing the Black Butte plagioclase phenocryst and microphenocryst core and microlite An-compositions. The two populations define distinct regions of compositional space with no overlap. Phenocryst and microphenocryst rim compositions are not plotted. Number in parentheses is the number of analyses used in the histogram. B. Plot of crystal width versus plagioclase An content. Phenocryst and microphenocryst core and microlite values are plotted. The two dashed lines denote the extent of microphenocryst (50–150 μm) and microlite (≤50 μm) width values. No rim compositions are shown on this plot. Some of the scatter in the phenocryst and microphenocryst data results from cut-section effect issues, i.e., the absolute variance in measurement declines as the crystal size declines.

not be directly measured in the Black Butte samples, an estimate of the melt composition, which crystallized to form the groundmass, was determined by mass balance. This method utilized measured modal analyses and phenocryst and bulk rock compositions. The average groundmass composition is plotted against the available data for all Shasta magma compositions (Fig. 3).

4.2. Geothermometry

The phenocryst crystallization temperature calculated for Black Butte using the silica-undersaturated plagioclase-amphibole geothermometer (Holland and Blundy, 1994) averages 896 °C (±40 °C) at 300 MPa. For this geothermometer to be applicable, plagioclase and amphibole must be co-crystallizing, equilibrium phases. At Black Butte this is evidenced by both intergrown plagioclase and amphibole phenocrysts and by the presence of inclusions of both minerals in phenocrysts of the other (Fig. 2H). Average plagioclase core compositions were calculated for use in the thermometer using data from plagioclase traverses, plagioclase phenocryst core analyses, and analyses of plagioclase crystals trapped inside amphibole grains. This average ($An_{77.5}$), believed to represent the most primitive plagioclase composition crystallized from the melt, was input into the geothermometer. Unlike the plagioclase, the Black Butte amphibole phenocrysts appear homogeneous. Any compositional variations that may have been recorded in the outer edge of the crystals have been subsequently destroyed by the decompression induced breakdown of the rim material. Given the compositional homogeneity of the amphibole phenocrysts, an average composition (Table 1) was input into the plagioclase-amphibole geothermometer. Additionally,

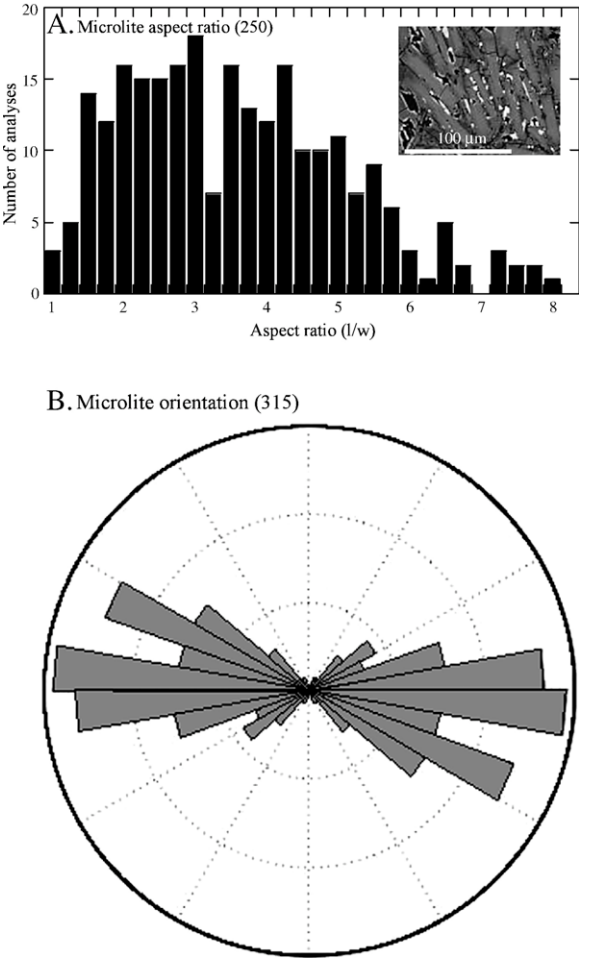

Fig. 8. A. Histogram of plagioclase microlite aspect ratio values. The majority of microlites are rectangular in shape to varying degrees. Number in parentheses is the number of analyses used in the histogram. B. Rose plot illustrating the strong orientation of plagioclase microlites. Number in parentheses is the number of analyses used in the plot.

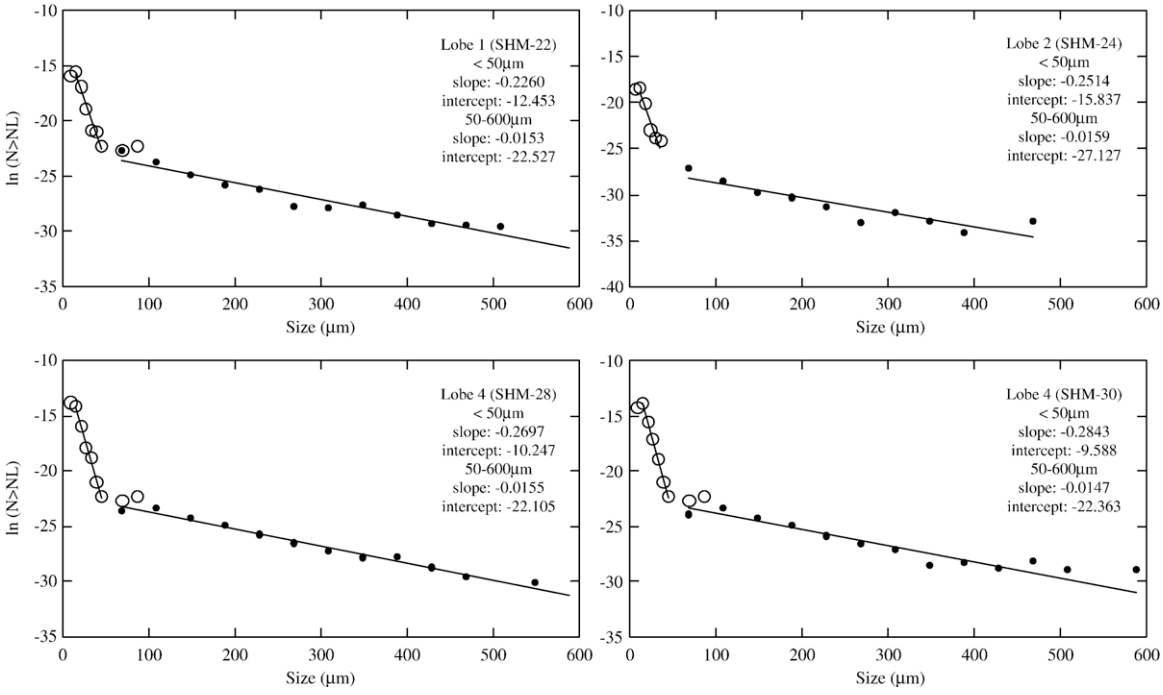

Fig. 9. Shape-corrected CSDs for the plagioclase phenocrysts, microphenocrysts, and microlites from various Black Butte locations showing two discrete populations. Population density, i.e., the number of crystals of different sizes in a unit volume, is referenced as (N>NL). Data for magnifications of 5× and 500× are plotted. Linear fits to the data are shown. Note the two distinct slopes and intercepts necessary to fit the data.

this geothermometer requires input of a pressure estimate. For the Black Butte samples 300 MPa was assumed, however the calculated temperature varies by only 8 °C for the pressure range 200 to 400 MPa.

4.3. Experimental phase equilibria

In order to more precisely determine the crystallization conditions of the Black Butte magma as recorded by the phenocryst core compositions, water-saturated experiments were performed over a range of T, P, and f_{O2} conditions (Fig. 10; Table 3). Although the lack of residual melt or intact melt inclusions precluded direct measurements of magmatic water content in the natural samples, it was assumed that the magma was likely close to water-saturated (i.e., $P_{total}=P_{H2O}$). Several lines of evidence suggest the melt was very water-rich. First, previous work by Baker et al. (1994) on the associated Mt. Shasta mafic samples measured water contents of 3–6 wt.% in the magmas. More evolved rocks from the same magmatic system should have similar or greater H_2O contents. Second, experiments have shown that 4–5 wt.% water is necessary to crystallize amphibole in a similar assemblage (pyroxene+amphibole+plagioclase+high-silica melt) equilibrated at a similar temperature and f_{O2} (Rutherford et al., 1985; Rutherford and Devine, 1988). Additionally, there is no clinopyroxene in the phase assemblage, indicating that not only was there sufficient water to stabilize amphibole, there was sufficient water to cause complete reaction of any pre-

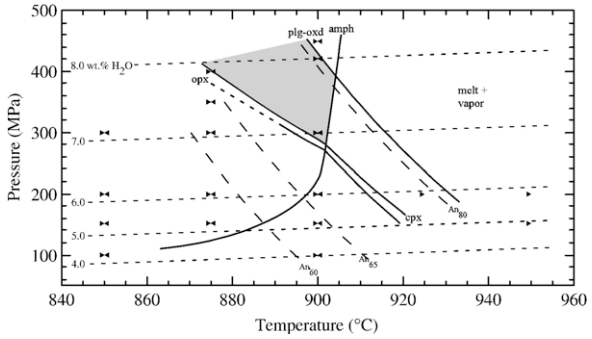

Fig. 10. Water-saturated phase diagram for SHAS-13 starting composition. Triangles denote experiments performed with their direction indicating forward or reverse experiments. Solid phase boundary lines are the phase-in lines for the named mineral (amph = amphibole, plg = plagioclase, cpx = clinopyroxene, opx = orthopyroxene, oxd = Fe–Ti oxide). Plagioclase anorthite compositions determined experimentally are represented by dashed compositional contours with An numbers next to them. Numbered small dashed lines are water concentration isopleths calculated using the water solubility model of Moore et al. (1998). The shaded region indicates the P–T space over which the Black Butte phase assemblage is stable.

Table 3
Representative experimental samples. Major element totals are recorded as oxide weight percent. Numbers in parantheses indicate one standard deviation

T (°C)	MC-69	MC-70	MC-68
	900	870	850
P (MPa)	300	300	300
Glass			
SiO_2 [a]	67.83 (0.53)	68.44 (0.40)	69.31(0.47)
TiO_2	0.38 (0.05)	0.42 (0.06)	0.33(0.03)
Al_2O_3	17.76 (0.15)	17.84 (0.20)	16.97(0.19)
FeO [b]	2.30 (0.27)	1.81 (0.13)	2.47(0.17)
MgO	0.80 (0.18)	0.98 (0.08)	0.83(0.05)
CaO	4.65 (0.15)	4.24 (0.12)	3.55 (0.08)
Na_2O	5.05 (0.28)	4.68 (0.14)	5.00 (0.22)
K_2O	1.19 (0.08)	1.52 (0.06)	1.47 (0.05)
MnO	0.04 (0.03)	0.07 (0.04)	0.07 (0.03)
Total	100.00	100.00	100.00
Plagioclase			
SiO_2	48.63 (0.48)	52.18 (0.45)	52.75 (0.52)
Al_2O_3	32.95 (0.44)	30.72 (0.47)	30.32 (0.10)
FeO [b]	0.45 (0.05)	0.14 (0.02)	0.36 (0.13)
CaO	15.74 (0.37)	12.82 (0.33)	12.58 (0.44)
Na_2O	2.43 (0.13)	3.84 (0.21)	4.01 (0.18)
K_2O	0.04 (0.01)	0.07 (0.02)	0.08 (0.01)
Total	100.24	99.77	100.10
An	76.1	62.2	60.6
Ab	23.5	37.2	38.6
Or	0.4	0.6	0.8
Amphibole			
SiO_2	46.72 (0.76)	47.31 (0.40)	45.83 (1.13)
TiO_2	1.68 (0.16)	1.70 (0.10)	1.78 (0.20)
Al_2O_3	10.52 (0.61)	10.39 (0.77)	10.36 (0.98)
FeO [b]	9.32 (0.94)	8.35 (0.55)	11.46 (0.68)
MgO	16.24 (0.82)	17.02 (0.38)	15.13 (0.36)
CaO	11.19 (0.24)	11.03 (0.40)	10.99 (0.40)
Na_2O	1.82 (0.14)	1.86 (0.12)	1.88 (0.15)
K_2O	0.19 (0.02)	0.19 (0.02)	0.21 (0.04)
MnO	0.10 (0.05)	0.13 (0.03)	0.14 (0.04)
Cr_2O_3	0.03 (0.03)	0.03 (0.03)	0.03 (0.03)
Total	97.81	98.01	97.81
Mg# [c]	76	71	70

[a] Glass totals normalized to anhydrous conditions.
[b] All Fe as FeO.
[c] Mg# calculated as $(Mg/(Mg+Fe^{2+}))*100$.

existing, high-temperature clinopyroxene to amphibole. Finally, the phenocryst assemblage, modal abundance, and mineral compositions were all replicated experimentally under water-saturated conditions.

To confirm the f_{O2} of the natural system, experiments were run buffered at f_{O2} values of NNO+1 and NNO+2. Oxygen fugacity has a strong effect on Fe–Mg equilibrium, therefore variations in the experimental f_{O2} have the greatest effect on mafic mineral crystallization (i.e., amphiboles and oxides for the Black Butte assemblage). At f_{O2} values ≤NNO, a majority of iron in the melt exists as Fe^{2+} (e.g., Kress and Carmichael, 1991). This results in Fe–Ti oxide crystallization being suppressed relative to other mafic mineral phases. As oxidation increases, the fraction of iron present as Fe^{3+} increases, resulting in an expansion of the stability field of Fe–Ti oxide crystallization at the expense of the Fe–Mg silicate minerals. This was evident in experimental runs at higher f_{O2} values (NNO+2), which resulted in early and extended Fe–Ti oxide crystallization and suppression of the appearance of amphibole on the liquidus. Experiments run at NNO+1 resulted in amphiboles with $Mg\#_{75}$ which is consistent with the average Black Butte amphibole $Mg\#_{77}$ (Table 3). The similar mafic mineral phase compositions indicate the experimental f_{O2} conditions replicate those of the natural system.

The phase equilibria for the Black Butte dacite under water-saturated conditions and at a f_{O2} of NNO+1 illustrate how mineral stability varies as a function of the experimental pressure and temperature conditions as well as f_{O2} (Fig. 10). Amphibole is the liquidus phase for this magma composition above 380 MPa; plagioclase is the liquidus phase at lower pressures. At 896 °C, the temperature calculated from amphibole-plagioclase phenocryst compositions, amphibole, plagioclase, and Fe–Ti oxides are stable from 300 MPa to <450 MPa. Plagioclase composition changes as a function of pressure and temperature (shown as compositional contours in Fig. 10), with high An plagioclase stable at higher pressures and temperatures and low An plagioclase stable at lower pressures and temperatures. Under lower pressure conditions (<220 MPa) clinopyroxene and orthopyroxene crystallize first rather than amphibole in a magma cooling at these pressures. This is evidenced in the natural samples by the presence of pyroxene crystals in the groundmass, but not as a phenocrystic phase. The shaded region in Fig. 10 indicates the region of phase space where the Black Butte phase assemblage and phenocryst composition would be stable (T=890–910 °C, P=≥300 MPa, f_{O2}=NNO+1, X_{H2O}=1). This temperature range overlaps that calculated using the amphibole–plagioclase geothermometer.

Modal analysis of the natural samples indicated the percentage of phenocrysts present in the Black Butte dacite at the time of eruption was 20±2% (Table 1). Fig. 11 illustrates the changing melt crystallinity as a function of temperature over a range of experimental pressures with $P_{total}=P_{H2O}$, calculated from the experimental glass data, the bulk magma composition, and the phase compositions. The crystallinity of the Black Butte dacite based on the modal abundance of phenocrysts is

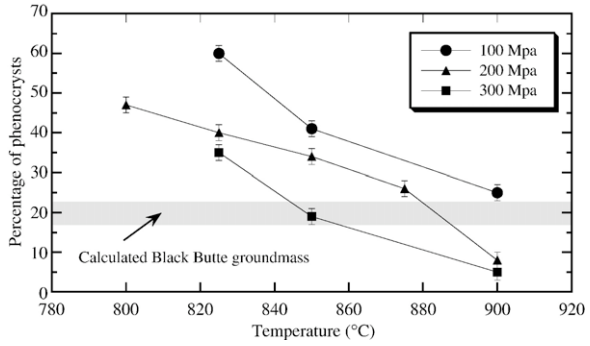

Fig. 11. Plot of temperature vs. experimental sample crystallinity at different P_{H2O}. The shaded region indicates the crystallinity of the Black Butte dacite at the time of eruption calculated using the point counting technique (Table 1). Error bars indicate one standard deviation.

shown for comparison. Assuming some phenocryst growth occurred during magma ascent, the phenocryst content at the maximum P–T conditions indicated by the phase equilibria experiments must have been less than 20%. If the phase equilibria constraint (Fig. 10) that indicates the Black Butte magma contained the observed high P–T assemblage (~An_{78} plagioclase + amphibole) at ≥300 MPa and 900 °C is accepted, the mass balance summary provided in Fig. 11 can be used to determine the crystallinity of the magma at this early stage. The crystallinity of this early melt is 5% for a pressure of 300 MPa. Plagioclase and amphibole phenocryst cores of the correct composition would crystallize in this region. The observation that this phenocryst abundance (5%) is lower than that measured in the natural samples (20%) is explained by a combination of crystal accumulation in the storage region and crystal coarsening. Potential processes that could produce the measured 20% phenocryst abundance, e.g., lowering the temperature, pressure, or P_{H2O}, would result in changes in crystal composition that would not replicate the natural samples.

The crystallinity contours indicate the magma would reach 20% crystallinity when the pressure was reduced to ~150 MPa (Fig. 11), assuming the ascent was approximately adiabatic, i.e., there was no significant temperature drop accompanying ascent. The stable plagioclase composition at this pressure is $An_{60–65}$ (Fig. 10). This is the composition where the microlites began to grow and is therefore consistent with the observation that crystallization beyond this point was largely controlled by nucleation and growth of groundmass phases.

Experimental matrix melt compositions vary with changing temperature and pressure (Fig. 12). Melt CaO and Al_2O_3 content decreases with decreasing temperature as plagioclase crystallization progresses. In contrast, melt SiO_2 and K_2O increase with decreasing temperature and are enriched in the residual melt as neither element is incorporated into the crystallizing phase assemblage in large amounts. The data also indicates that at constant

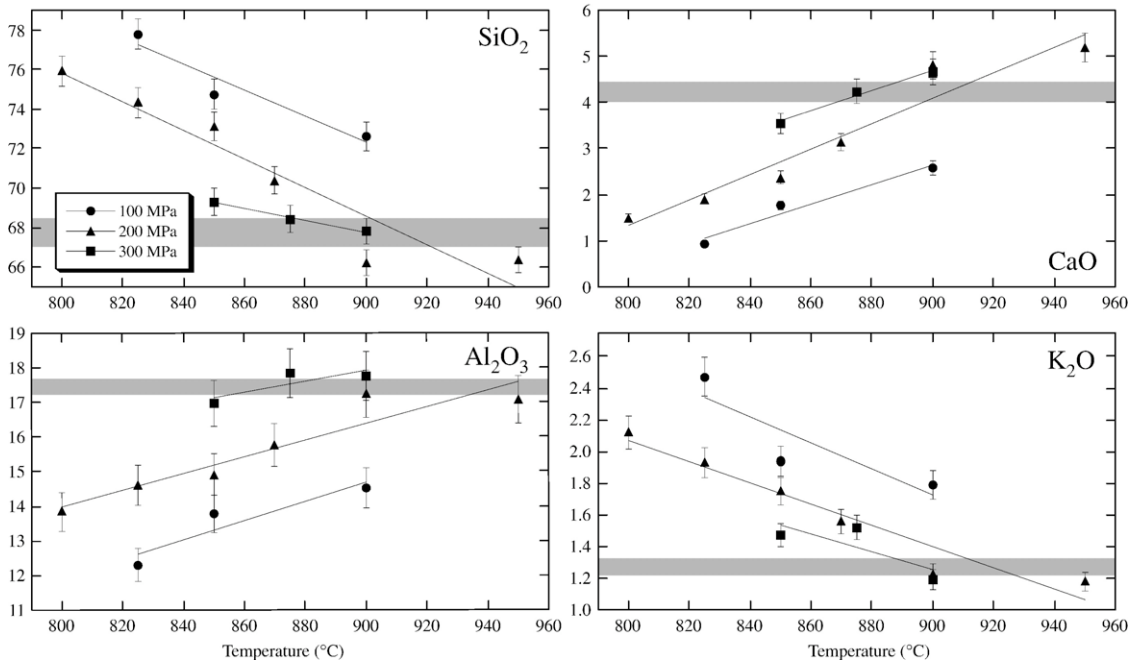

Fig. 12. Plot of temperature vs. experimental melt composition for a range of pressure values. The shaded region in each plot indicates the calculated Black Butte groundmass composition given in Table 1.

temperature the melt CaO and Al_2O_3 contents decrease with decreasing pressure due primarily to the onset and continuous crystallization of plagioclase. These changes in the melt composition also reflect changes in the plagioclase composition (Figs. 10 and 12). The chemical composition of the Black Butte matrix melt, inferred from mass balance as described above, is replicated experimentally under P–T conditions similar to those under which the phenocryst population is replicated (T=900±40 °C, 200–300 MPa).

5. Discussion

5.1. Relationship to the Mount Shasta magmatic system

Black Butte has a clear relationship to Mount Shasta, specifically to the Shastina dome which forms part of the summit of Shasta and which is believed on the basis of stratigraphic evidence and radiocarbon dating to have erupted contemporaneously with Black Butte (Miller, 1978). In addition to its geographic position, bulk rock samples from Black Butte and Shastina have similar major, minor, and trace element compositions (Table 1). However, these two lavas contain different phenocrystic phase assemblages. Black Butte is composed only of amphibole, plagioclase, and minor Fe–Ti oxides, whereas Shastina is composed of low-Ca and high-Ca pyroxene, amphibole, plagioclase, and minor Fe–Ti oxides. This difference in mafic mineral assemblage suggests that the equilibrium conditions the two magmas experienced during crystallization were different. As the bulk rock compositions of Black Butte and Shastina are chemically similar, the phase equilibria experiments from this study can also be applied to Shastina. The presence of phenocrystic high and low-Ca pyroxene and lower plagioclase An content (cores= $An_{56\pm6}$) indicate that either the Shastina magma crystallized at lower pressure and temperature than that of Black Butte (Fig. 10) or under conditions with $P_{H2O}<P_{total}$. Based on plagioclase composition and experimental data, Grove et al. (2005) concluded the Shastina magmas crystallized under water-saturated conditions at ~200 MPa, a significantly lower pressure than determined for the Black Butte magmas.

5.2. Amphibole breakdown rims and magma ascent rate

Utilizing decompression experiments run on Black Butte dacites and on compositionally similar dacites from Mount St. Helens (Rutherford and Hill, 1993), the amphibole decompression breakdown rim widths measured at Black Butte can be interpreted in terms of magma ascent rate. The overall range of rim widths measured (19–59 μm) correspond to a time-integrated ascent rate of 0.004–0.006 m/s from the depth where amphibole became unstable (with an average pressure of 200 MPa applied) to the surface. The magma ascent rates calculated from the Black Butte amphibole reaction are in the range of ascent rates determined for other volcanic centers involving effusive eruptions (Table 4).

The dynamics of dome-forming eruptions have been studied in great detail recently as a result of the 1980–86 extrusions at Mount St. Helens, the 1991–95 eruptions at Mount Unzen, Japan, and the 1995-present eruptions at Soufriere Hills, Montserrat. Magma ascent rates, as calculated using the width of amphibole reaction rims, have been found to vary over the course of an eruption in at least two of these cases. At Mt. St. Helens, the cryptodome magma emplaced just before the May 18, 1980 explosive event contained amphibole phenocrysts all with a thin (<6 μm) reaction rim. Based on this evidence the magma samples studied were interpreted as rapidly emplaced (Rutherford and Hill, 1993). In the explosive event of May 18, the erupted magma contained amphiboles that had ascended so rapidly that they were completely unrimmed. However, in all dome samples subsequently erupted, thick-rimmed amphiboles were found to coexist with the main population of thin-rimmed amphiboles in the same sample. This resulted in rim-width histograms with a distinct peak followed by a long tail of thicker rim widths, interpreted as evidence of fast moving magma pulses from the storage zone entraining older magmas lining the conduit walls (Rutherford and Hill, 1993). A similar set of observations was made for some eruptions of the 1995–2003 Soufriere Hills andesite, Montserrat, specifically when dome growth was low (Rutherford and Devine, 2003). For this system, ascent rates, measured using amphibole reaction rim thickness, were seen to vary throughout the eruption with thin or unrimmed phenocrysts appearing during periods where

Table 4
Extrusive ascent rate comparisons. Ascent rates for volcanoes other than Black Butte from Geschwind and Rutherford (1995) (St. Helens), Rutherford and Hill (1993) (St. Helens), Rutherford and Devine (2003) (Soufriere Hills), Venezky and Rutherford (1999) (Unzen)

Volcano	Measurement method	Ascent rate (m/s)	Magma type
St. Helens	Groundmass crystallization	0.01–0.02	Dacite
St. Helens	Amphibole rims	0.004–0.015	Dacite
Soufriere Hills	Amphibole rims	0.001–0.02	Andesite
Unzen	Magnetite zonation	0.002	Dacite
Black Butte	Amphibole rims	0.004–0.006	Dacite

volcanic explosions in the vent were common (Rutherford et al., 1998). It appears that the gas exsolved during ascent was not able to escape from the more rapidly ascending magmas. Closed-system degassing gave rise to the explosive behavior (Voight et al., 1999). In contrast to amphibole rim widths in the Mt. St. Helens 1980 dacites, which ranged from 0–60 μm in single thin sections (Rutherford and Hill, 1993), the domes at Black Butte show little variability in amphibole rim widths within a given sample (Fig. 5A) suggesting that remobilization of older magmas lining the conduit was not an important process during the Black Butte eruption. However, there is a range in rim widths in different Black Butte samples from the same dome lobe and from lobe to lobe (Fig. 5A–E) indicating variations in magma ascent rate that range from 0.004–0.006 m/s. Also of interest is the lack of unrimmed amphiboles identified in the Black Butte magmas. This indicates that none of the sampled Black Butte magmas rose rapidly enough to avoid amphibole breakdown. As seen at Mt. St. Helens and Montserrat, unrimmed amphiboles are generally associated with explosive eruptions. The lack of unrimmed material in the sampled Black Butte rocks is consistent with the fact that no evidence of explosive activity is found associated with this eruptive event. Apparently, ascent of this magma was slow enough for complete volatile exsolution leading to an effusive, not explosive, eruption at Black Butte.

A distinct peak in rim width values occurs at 34 ± 10 μm, with a majority of rim widths falling within this narrow range, implying a similar ascent rate between dome lobes. The slightly greater rim widths evident in lobes 1 and 4 (Fig. 5B, E) correspond to slightly slower ascent rates, but do not measurably change the calculated rate of 0.004–0.006 m/s. This time-integrated ascent rate suggests the magma rose at approximately the same rate as each lobe was emplaced. If the magma experienced multiple episodes of extrusion or if there were significant pauses in the conduit flow, cooling through the conduit margins would have resulted in a stagnant magma along the walls that could have been remobilized later. This type of extrusion would have produced amphibole phenocrysts with both thick and thin rims coexisting in the same sample as seen at Mount St. Helens, but not evident in the Black Butte magmas. Thus, the Black Butte eruption appears to represent a single magma mobilization and flow event. The more pronounced variability in ascent rates (rim thickness range) during emplacement of the initial (lobe 1) and final (lobe 4) eruptive products seems a logical reflection of the beginning and waning stages of the eruption.

5.3. Plagioclase growth kinetics

In addition to the homogeneous amphibole breakdown rim widths, the compositional gap between the plagioclase phenocryst and microlite core populations and the crystal size distribution data also suggest a slow, continuous magma ascent rate. The gap in plagioclase composition and the break in slope of the CSD plot suggest two growth regimes were present in the Black Butte magma (Figs. 7A and 9). The high-An contents of large homogeneous plagioclase phenocryst cores indicate they crystallized at pressures of ≥300 MPa (Fig. 10) probably at low degrees of undercooling. The phenocryst content of the magma was estimated above to be 5 vol.% at this stage. The surrounding normally zoned rims of progressively lower-An plagioclase are the result of decompression-induced crystallization of the H_2O-rich melt. These rims span the compositional range from $An_{77.5}$ to $An_{39.8}$. This corresponds to equilibrium crystallization along an adiabat from ~400 MPa to <100 MPa (Fig. 10). The small population of relict sieve-cored phenocrysts that are present also exhibit thick mantles of high-An content and rims similar in compositional range to the clear plagioclases. This indicates that despite a prior history, potentially in the greater Shasta magmatic system, these sieve-cored plagioclase phenocrysts share a common crystallization path with the main population of plagioclase phenocrysts in the Black Butte magmas.

As decompression began, plagioclase phenocrysts were mantled by rims of progressively lower An content. This growth continued throughout the ascent process resulting in the normally zoned rims observed. If it is assumed that the 15–20 μm rims present on all the phenocrysts grew during ascent from the equilibration depth of ≥300 MPa and that the ascent rate calculated from the amphibole breakdown rims was constant, then a maximum plagioclase phenocryst growth rate of 8.7×10^{-8} mm/s for the rim material is calculated. This growth rate is comparable to plagioclase growth rates from other studies of silicic melts undergoing decompression-induced crystallization (Table 5) (Cashman, 1992; Hammer and Rutherford, 2002; Izbekov et al., 2002; Larsen, 2005).

In contrast to the high An values measured in the plagioclase phenocryst cores, no compositions with An contents greater than $An_{62.0}$ were measured in the plagioclase microlite population (defined as having widths ≤50 μm) (Fig. 7A). In addition, size distribution data clearly shows two distinct populations of plagioclase in the Black Butte magma (Fig. 9). The presence of two plagioclase populations as well as the compositional disparity between the two populations suggests that

Table 5
Plagioclase growth rate. Growth rates for samples other than Black Butte from Larsen (2005), Izbekov et al. (2002), Cashman (1992), and Couch (2003)

Location	Crystal type	Growth rate (mm/s)	Melt type
Black Butte	Phenocryst rims	8.7×10^{-8}	Dacite
Black Butte	Microlites	2.5×10^{-8}	Dacite
Aniakchak	Phenocryst rims	3.5×10^{-9}–60.6×10^{-9}	Rhyodacite
Aniakchak	Microlites	4.4×10^{-9}–65.7×10^{-9}	Rhyodacite
Karymsky	Phenocryst rims	2.5×10^{-9}	Andesite
Mount St. Helens	Microlites	1–3×10^{-10}	Dacite
Synthetic	Microlites	7.69×10^{-9} -1.14×10^{-7}	Haplogranite (73 wt.% SiO_2)

measurable microlite growth was not recorded (i.e., high-An cores) until significantly into the ascent process (Fig. 10) when low-An plagioclase ($<An_{65}$) was stable.

By assuming that the decompression rate determined by amphibole breakdown rims was constant throughout ascent and that the microlites began to grow at pressures of ~150 MPa (from the phase equilibria experiments), microlite growth rates were calculated for the ten largest microlites using the half-crystal growth rate method described by Hammer and Rutherford (2002) [$(LW)^{0.5}/(2t)$, where L and W are the measured length and width and t is the ascent time]. This yields an average growth rate of 2.5×10^{-8} mm/s (Table 5). Comparison of the Black Butte microlites rates with the phenocryst rim growth rate above suggests that the two grew at comparable rates.

The compositional variations in the plagioclase population and the two crystal populations viewed in the size distribution data provide strong evidence for two distinct episodes of crystallization, one in the magma storage region and one during magma ascent (Figs. 10 and 13). This process of syneruptive crystallization is also thought to have played a role in other volcanic systems, i.e., Mount St. Helens (Blundy and Cashman, 2005), Merapi (Hammer et al., 2000), and Montserrat (Couch et al., 2003). The experimental data indicates that the homogeneous, unzoned, high An phenocryst cores can only have grown at depth (Fig. 10). The phenocryst and microphenocryst rims and the microlites, both of which have significantly lower An values could not have crystallized at depths similar to those of the phenocryst cores, and therefore grew over a range of lower pressures. This suggests that two crystal growth regimes were present at Black Butte, one in the magma storage region and one in the magma conduit. Additionally, the correlation between width and An content strengthens the assertion that the microlite population had significantly less time to grow than the phenocryst population thereby suggesting they grew late in the magmas history (Fig. 7B). The compositionally unzoned character of the amphiboles and the plagioclase inclusions within the amphiboles suggests the amphibole cores grew uniformly at depth ($P\geq300$ MPa). Any changes in amphibole composition with ascent have been overprinted by the breakdown products now completely rimming the crystals.

5.4. Black Butte eruptive model

The main objective in determining the phase equilibria of the Black Butte dacite magma was to be able to use this data in conjunction with composition and texture in the natural samples to assess magma ascent dynamics during eruption of the Black Butte magma (Fig. 13). This study has quantified the extent of three crystallization processes occurring in the Black Butte dacite that can be used to discern ascent processes. These indicators are active over different, but sometimes overlapping, regions of decompression history. First, plagioclase phenocryst rim growth or overgrowth appears to have occurred continuously with decreasing pressure from depths of ≥300 MPa. Second, amphibole rim growth due to decompression-induced breakdown began at ~200 MPa (Fig. 10) and continued throughout the remaining magma ascent. Finally, a delay between the start of decompression and the nucleation and growth of a distinct plagioclase crystal population is suggested by the compositions and textures of groundmass crystals. If an adiabatic ascent path is assumed for the Black Butte magma, the microlites did not begin to form until pressures of ~150 MPa were reached (Fig. 10). Although some heating as a result of the release of the heat of crystallization is possible during ascent, there is no way to assess this effect in the upper conduit and any thermal effect is certain to have been offset by the loss of heat due to volatile exsolution. Each of these three observations yield constraints on the kinetics of magma ascent at Black Butte (Fig. 13) and suggest that ascent was a slow process.

Several additional factors support the argument for a slow, continuous magma ascent. The first is the equant shape of the plagioclase microlite population as well as the presence of normal zonation in the largest of the microphenocrysts. Hammer and Rutherford (2002) report that planar faceted crystals exhibiting normal zonation, such as those seen in the Black Butte dacite, are indicative of slow decompression. Additionally, the

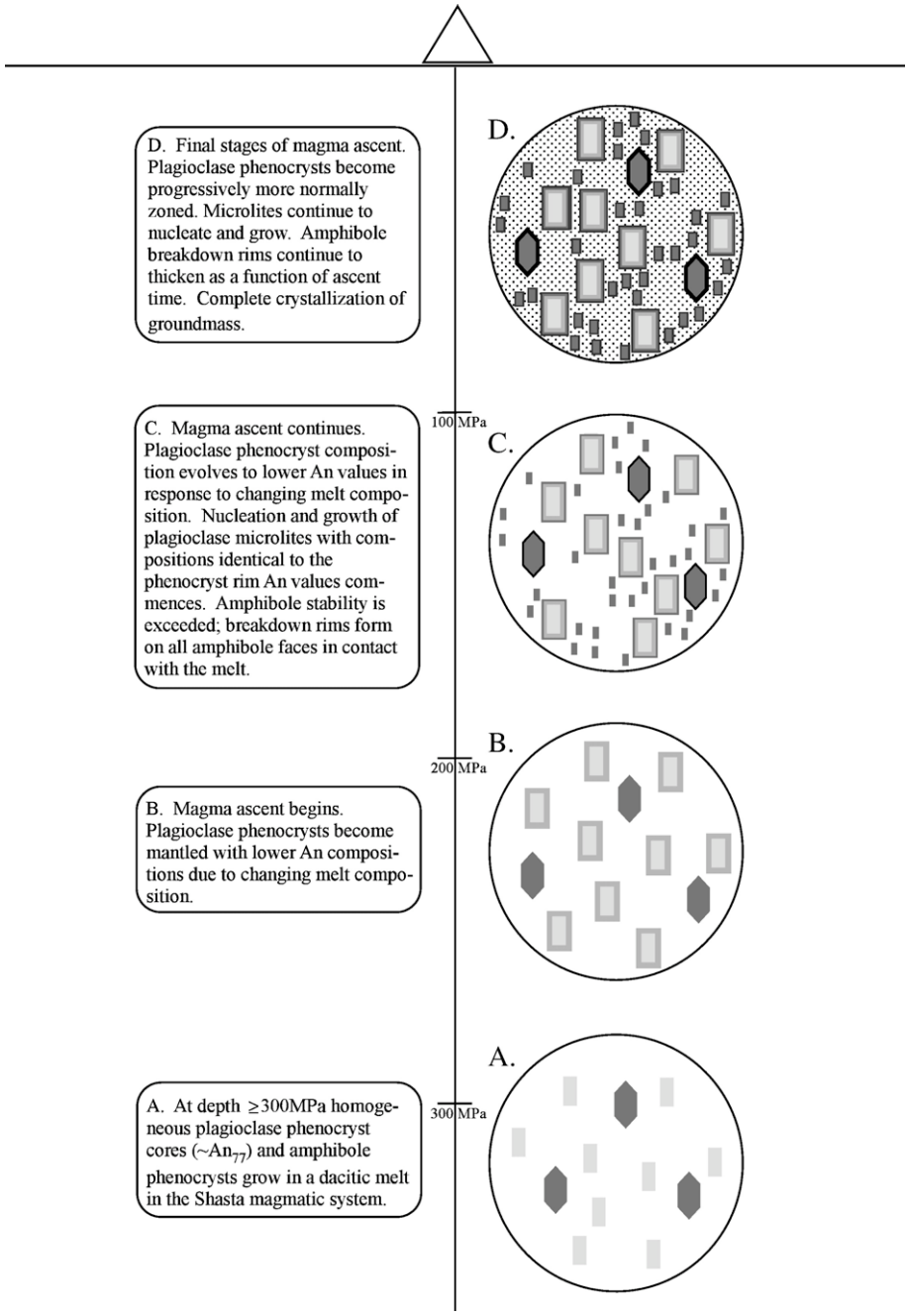

Fig. 13. Idealized illustration of the compositional changes taking place during the crystallization and ascent processes at Black Butte. Hexagonal crystals represent amphibole; rectangular crystals represent plagioclase. Both compositional and breakdown rims formed during ascent are portrayed by darker material. Final complete groundmass crystallization is represented by the stippled pattern in D.

strong crystal fabric present in the microlites indicates a laminar flow regime (Castro et al., 2002), which is also consistent with the petrologic indicators of slow ascent. The second factor is the near complete crystallization of the interstitial melt in all samples. This implies a slow ascent and/or extrusion to allow time for the crystallization of all available melt. The final factor is the general absence of any pumiceous Black Butte samples. The paucity of vesicles in these rocks indicates that the ascent and/or extrusion times were slow enough to allow extensive magma degassing. In contrast, the Mount St. Helens and Montserrat eruptions also produced lava

domes, but in both cases there were several explosive volcanic events as well (Rutherford et al., 1998; Sparks et al., 1998) that produced widespread highly vesiculated ash and pumice blocks. These events followed an increase in magma ascent rate, as calculated from amphibole reaction rims, suggesting that the melts had insufficient time to degas (Rutherford et al., 1998; Voight et al., 1999). Based on the experimental phase equilibria, the uniformity of the amphibole reaction rims, and the plagioclase phenocryst and microlite compositions and size distributions, Black Butte appears to represent a magma that crystallized its phenocryst population of plagioclase and amphibole at depth, subsequently was separated from the main Shasta magma storage region, and traveled to the surface in a slow, continuous flow without any significant pauses or mixing events with previous magmas lining the conduit (Fig. 13). Any explosive events must have occurred early and may have been covered by subsequent voluminous eruptive products from Shasta as no explosive material from this vent has been identified.

Acknowledgements

This research was supported by the National Science Foundation grant EAR-0309870 to M.J.R. and the U.S. Geological Survey Jack Kleinman Memorial Research Fellowship to M.C.M. The authors wish to thank Drs. J. Devine and C. Mandeville for their assistance with electron microprobe analyses and C. Daigle for her help in the field. Constructive reviews by Drs. J. Brophy and A. Conte were greatly appreciated.

References

Bacon, C.R., Bruggman, P.E., Christiansen, R.L., Clynne, M.A., Donnelly-Nolan, J.M., Hildreth, W., 1997. Primitive magmas at five Cascade volcanic fields: melts from hot, heterogeneous sub-arc mantle. Canadian Mineralogist 35, 397–423.

Baker, M.B., Grove, T.L., Price, R., 1994. Primitive basalts and andesites from the Mt. Shasta region, N. California: products of varying melt fraction and water content. Contributions to Mineralogy and Petrology 118, 111–129.

Blundy, J., Cashman, K.V., 2001. Ascent-driven crystallization of dacite magmas at Mount St. Helens, 1980–86. Contributions to Mineralogy and Petrology 140, 631–650.

Blundy, J., Cashman, K.V., 2005. Rapid decompression-driven crystallization recorded by melt inclusions from Mount St. Helens volcano. Geology 33, 793–796.

Browne, B.L., Gardner, J.E., 2004. The nature and timing of caldera collapse as indicated by accidental lithic fragments from the ~1000 A.D. eruption of Volcan Ceboruco, Mexico. Journal of Volcanology and Geothermal Research 130, 93–105.

Cashman, K.V., 1992. Groundmass crystallization of Mount St. Helens dacite, 1980–1986: a tool for interpreting shallow magmatic processes. Contributions to Mineralogy and Petrology 109, 431–439.

Castro, J., Manga, M., Cashman, K., 2002. Dynamics of obsidian flows inferred from microstructures: insights from microlite preferred orientations. Earth and Planetary Science Letters 199, 211–226.

Condie, K.C., Swenson, D.H., 1974. Compositional variation in three Cascade stratovolcanoes; Jefferson, Rainier, and Shasta. Bulletin of Volcanology 37, 205–230.

Couch, S., 2003. Experimental investigation of crystallization kinetics in a haplogranite system. American Mineralogist 88, 1471–1485.

Couch, S., Harford, C.L., Sparks, R.S.J., Carroll, M.R., 2003. Experimental constraints on the conditions of formation of highly calcic plagioclase microphenocrysts at Soufriere Hills Volcano, Montserrat. Journal of Petrology 44, 1455–1475.

Eugster, H.P., 1957. Heterogeneous reactions involving oxidation and reduction at high pressures and temperatures. Journal of Chemical Physics 26, 1760.

Eugster, H.P., 1959. Oxidation and reduction in metamorphism. In: Abelson, P.H. (Ed.), Researches in Geochemistry. John Wiley and Sons, New York, pp. 397–426.

Eugster, H.P., Skippen, G.B., 1967. Igneous and metamorphic reactions involving gas equilibria. In: Abelson, P.H. (Ed.), Researches in Geochemistry, vol. 2. John Wiley and Sons, New York, pp. 492–520.

Frost, B.R., 1991. Introduction to oxygen fugacity and its petrologic importance. In: Lindsley, D.C. (Ed.), Oxide Minerals. Mineralogical Society of America, Washington, D.C., pp. 1–9.

Garcia, M.O., Jacobson, S.S., 1979. Crystal clots, amphibole fraction and the evolution of calc-alkaline magmas. Contributions to Mineralogy and Petrology 69, 319–327.

Geschwind, C.-H., Rutherford, M.J., 1992. Cummingtonite and the evolution of the Mount St. Helens (Washington) magma system: an experimental study. Geology 20, 1011–1014.

Geschwind, C.-H., Rutherford, M.J., 1995. Crystallization of microlites during magma ascent: the fluid mechanics of 1980–1986 eruptions at Mount St. Helens. Bulletin of Volcanology 57, 356–370.

Grove, T.L., Baker, M.B., Price, R.C., Parman, S.W., Elkins-Tanton, L.T., Chatterjee, N., Müntener, O., 2005. Magnesian andesite and dacite lavas from Mt. Shasta, northern California: products of fractional crystallization of H_2O-rich mantle melts. Contributions to Mineralogy and Petrology 148, 542–565.

Hammer, J.E., Rutherford, M.J., 2002. An experimental study of the kinetics of decompression-induced crystallization in silicic melt. Journal of Geophysical Research 107, ECV8-1–ECV8-24.

Hammer, J.E., Rutherford, M.J., 2003. Petrologic indicators of preeruption magma dynamics. Geology 31, 79–82.

Hammer, J.E., Cashman, K.V., Hoblitt, R.P., Newman, S., 1999. Degassing and microlite crystallization during pre-climactic events of the 1991 eruption of Mt. Pinatubo, Philippines. Bulletin of Volcanology 60, 355–380.

Hammer, J.E., Cashman, K.V., Voight, B., 2000. Magmatic processes revealed by textural and compositional trends in Merapi dome lavas. Journal of Volcanology and Geothermal Research 100, 165–192.

Hammer, J.E., Rutherford, M.J., Hildreth, W., 2002. Magma storage prior to the 1912 eruption at Novarupta, Alaska. Contributions to Mineralogy and Petrology 144, 144–162.

Holland, T., Blundy, J., 1994. Non-ideal interactions in calcic amphiboles and their bearing on amphibole–plagioclase thermometry. Contributions to Mineralogy and Petrology 116, 433–447.

Izbekov, P.E., Eichelberger, J.C., Patino, L.C., Vogel, T.A., Ivanov, B.V., 2002. Calcic cores of plagioclase phenocrysts in andesite from Karymsky volcano: evidence for rapid introduction by basaltic replenishment. Geology 30, 799–802.

Kress, V., Carmichael, I.S.E., 1991. The compressibility of silicate liquids containing Fe_2O_3 and the effect of composition, temperature, oxygen fugacity, and pressure on their redox states. Contributions to Mineralogy and Petrology 108, 82–92.

Larsen, J.F., 2005. Experimental study of plagioclase rim growth around anorthite seed crystals in rhyodacitic melt. American Mineralogist 90, 417–427.

Lawson, C.A., Nord Jr., G.L., Champion, D.E., 1987. Fe–Ti oxide mineralogy and the origin of normal and reverse remnant magnetization in dacitic pumice blocks from Mt. Shasta, California. Physics of the Earth and Planetary Interiors 46, 270–288.

Leake, B.E., Woolley, A.R., Arps, C.E.S., Birch, W.D., Gilbert, M.C., Grice, J.D., Hawthorne, F.C., Kato, A., Kisch, H.J., Krivovichev, V.G., Linthout, K., Laird, J., Mandarino, J.A., Maresch, W.V., Nickel, E.H., Rock, N.M.S., Schumacher, J.C., Smith, D.C., Stephenson, N.C.N., Ungaretti, L., Whittaker, E.J.W., Youzhi, G., 1997. Nomenclature of amphiboles: report of the subcommittee on amphiboles of the international mineralogical association, commission on new minerals and mineral names. American Mineralogist 82, 1019–1037.

Le Bas, M.J., Le-Maitre, R.W., Streckeisen, A., Zanettin, B.A., 1986. Chemical classification of volcanic rocks based on the total alkali-silica diagram. Journal of Petrology 27, 745–750.

Marsh, B.D., 1988. Crystal size distribution (CSD) in rocks and the kinetics and dynamics of crystallization I. Theory. Contributions to Mineralogy and Petrology 99, 277–291.

Miller, C.D., 1978. Holocene pyroclastic-flow deposits from Shastina and Black Butte, west of Mount Shasta, California. U.S. Geological Society J. Res., vol. 6, pp. 611–624.

Moore, G.M., Vennemann, T., Carmichael, I.S.E., 1998. An empirical model for the solubility of water in magmas to 3 kilobars. American Mineralogist 83, 36–42.

Nielsen, C.H., Sigurdsson, H., 1981. Quantitative methods of electron microprobe analysis of sodium in natural and synthetic glasses. American Mineralogist 66, 547–552.

Pallister, J.S., Hoblitt, R.P., Meeker, G.P., Knight, R.J., Siems, D.F., 1996. Magma mixing at Mount Pinatubo: petrographic and chemical evidence from the 1991 deposits. In: Newhall, C.G., Punonbgayan, R.S. (Eds.), Fire and Mud; Eruptions and Lahars of Mount Pinatubo, Philippines. University of Washington Press, Seattle, pp. 687–731.

Pichavant, M., Martel, C., Bourdier, J.-L., Scaillet, B., 2002. Physical conditions, structure, and dynamics of a zoned magma chamber; Mount Pelee (Martinique, Lesser Antilles arc). Journal of Geophysical Research 107, ECV 1-1.

Robinson, P., Spear, F.S., Schumacher, J.C., Laird, J., Klein, C., Evans, B.W., Doolan, B.L., 1982. Phase relations of metamorphic amphiboles: natural occurrence and theory. In: Veblen, D.R., Ribbe, P.H. (Eds.), Amphiboles: petrology and experimental phase relations. Mineralogical Society of America, Washington, D.C., pp. 1–22.

Rutherford, M.J., Devine, J.D., 1988. The May 18, 1980, eruption of Mount St. Helens 3. Stability and chemistry of amphibole in the magma chamber. Journal of Geophysical Research 93, 11949–11959.

Rutherford, M.J., Devine, J.D., 2003. Magmatic conditions and magma ascent as indicated by hornblende phase equilibria and reactions in the 1995–2002 Soufriere Hills magma. Journal of Petrology 44, 1433–1453.

Rutherford, M.J., Hill, P.M., 1993. Magma ascent rates from amphibole breakdown: an experimental study applied to the 1980–1986 Mount St. Helens eruptions. Journal of Geophysical Research 98, 19667–19685.

Rutherford, M.J., Sigurdsson, H., Carey, S., Davis, A., 1985. The May 18, 1980, eruption of Mount St. Helens 1. Melt composition and experimental phase equilibria. Journal of Geophysical Research 90, 2929–2947.

Rutherford, M.J., Devine, J.D., Barclay, J., 1998. Changing magma conditions and ascent rates during the Soufriere Hills eruption on Montserrat. GSA Today 8, 1–7.

Smith, A.L., Carmichael, I.S.E., 1968. Quaternary lavas from the southern Cascades, western USA. Contributions to Mineralogy and Petrology 19, 212–238.

Sparks, R.S.J., Young, S.R., Barclay, J., Calder, E.S., Cole, P., Darroux, B., Davies, M., Druitt, T.H., Harford, C., Herd, R., James, M., Lejeune, A.M., Norton, G., Skerrit, G., Stasiuk, M.V., Stevens, N.S., Toothill, J., Wadge, G., Watts, R., 1998. Magma production and growth of the lava dome of the Soufriere Hills Volcano, Montserrat, West Indies: November 1995 to December 1997. Geophysical Research Letters 25, 3421–3424.

Tsuchiyama, A., 1985. Dissolution kinetics of plagioclase in the melt of the system diopside–albite–anorthite, and origin of dusty plagioclase in andesites. Contributions to Mineralogy and Petrology 89, 1–16.

Venezky, D.Y., Rutherford, M.J., 1999. Petrology and Fe–Ti oxide reequilibration of the 1991 Mount Unzen mixed magma. Journal of volcanology and Geothermal Research 89, 213–230.

Voight, B., Sparks, R.S.J., Miller, A.D., Stewart, R.C., Hoblitt, R.P., Clarke, A., Ewart, J., Aspinall, W.P., Baptie, B., Calder, E.S., Cole, P., Druitt, T.H., Hartford, C., Herd, R.A., Jackson, P., Lejeune, A.M., Lockhart, A.B., Loughlin, S.C., Luckett, R., Lynch, L., Norton, G.E., Robertson, R., Watson, I.M., Watts, R., Young, S.R., 1999. Magma flow instability and cyclic activity at Soufriere Hills volcano, Montserrat, British West Indies. Science 283, 1138–1142.

Williams, H., 1932. Mount Shasta, a Cascade volcano. Journal of Geology 40, 417–429.